Mon. Not. R. astr. Soc. (1988) **232,** 381–406

An objective prism Hα survey of nearby clusters of galaxies – I. Abell 347 and Abell 1367

C. Moss* *Institute of Astronomy, Madingley Road, Cambridge, CB3 0HA*

M. Whittle* *Department of Astronomy, University of Virginia, Charlottesville, VA 22903, USA*

M. J. Irwin *Institute of Astronomy, Madingley Road, Cambridge, CB3 0HA*

Accepted 1987 November 19. Received 1987 November 17; in original form 1987 September 2

Summary. Using the Burrell Schmidt telescope equipped with a 10° objective prism and IIIaF emulsion we have made a high dispersion (~400 Å mm^{-1}) survey for Hα emission in galaxies in the two nearby rich clusters, Abell 347 and Abell 1367. We detect a total of 69 galaxies in Hα emission. Approximately 20 per cent of CGCG galaxies are detected, whilst 35 per cent of detected galaxies are fainter than the CGCG magnitude limit. All potentially detectable (cz<12 000 km s^{-1}) Markarian and Wasilewski galaxies in the cluster fields are recovered, and 60–80 per cent of potentially detectable *IRAS* galaxies are also recovered. The Hα+[N II] detection limits are difficult to define, but approximate flux and equivalent width thresholds are ~10^{-13} erg cm^{-2} s^{-1} and ~20 Å respectively. The digitized plates were used to determine global Hα+[N II] equivalent widths and fluxes. These measurements are in good agreement with values obtained for a small subset of galaxies measured using wide aperture photoelectric photometry. From a single plate an approximate redshift estimate may be made with (1σ) accuracy of ~550 km s^{-1}, by measuring the position of the Hα emission feature relative to the peak of the continuum spectrum. Using two prism plates taken with opposite dispersion directions, a more reliable redshift measurement may be made with (1σ) accuracy of ~200 km s^{-1}.

We will use the results from these two and other clusters to investigate environmental influences on global star formation rates in cluster galaxies.

1 Introduction

In order to understand both cluster and galaxy evolution, it is necessary to evaluate the relative importance of primordial conditions of galaxy formation and subsequent processes of environ-

* Visiting astronomer, Kitt Peak National Observatory, National Optical Astronomy Observatories, operated by the Association of Universities for Research in Astronomy, Inc. under contract with the National Science Foundation.

mental modification in the evolutionary history of a galaxy. One question of particular importance is the effect of the cluster environment upon the evolution of spiral galaxies. There is growing evidence for systematic differences between spirals in clusters and spirals in the field. These include a lower H I content for spirals in clusters (Giovanelli & Haynes 1985) and also a lower detection frequency of nuclear emission (Gisler 1978; Dressler, Thompson & Schectman 1985). Although these differences might lead one to suspect that spirals in clusters have a lower average star formation rate than spirals in the field, a comparison of cluster and field spirals by Kennicutt, Bothun & Schommer (1984) using Hα observations of global (disc plus nuclear) emission for selected spirals in three clusters shows no such effect, and in fact all three clusters contain several galaxies with unusually strong Hα emission. Moreover a recent radio survey of the Coma supercluster by Gavazzi & Jaffe (1985, 1986) shows enhanced star formation in cluster spirals. Clearly, further observations of the star formation rates in cluster spirals are of great interest.

One indicator of current massive star formation is the global Hα+ [N II] emission* (Kennicutt & Kent 1983), which may also be used to obtain quantitative estimates of the total star formation rate (Kennicutt 1983). It may be noted that nuclear spectroscopic observations alone do not provide reliable estimates of the global emission (Kennicutt & Kent 1983; Kennicutt *et al.* 1987). The usual technique for measuring global Hα emission has been wide-aperture photoelectric photometry of individual galaxies. Although this technique achieves a low detection threshold and high accuracy, it is relatively time-consuming and requires prior knowledge of the galaxy redshift. So far, measurements have been made for a limited sample of galaxies in a few clusters (Kennicutt *et al.* 1984). An alternative method to detect global Hα emission is to use a Schmidt telescope with a high-dispersion objective prism and IIIaF plates (Kinman 1979). This technique offers the possibility of surveying more rapidly and more efficiently a much larger sample of galaxies in nearby rich clusters. It also allows quantitative measurement of the Hα+[N II] equivalent width and flux, and radial velocity of the emission-line galaxies.

The above method of high-dispersion objective prism spectroscopy has been applied to two nearby rich clusters, Abell 347 and Abell 1367. The survey technique is described, and detected emission-line galaxies listed in Section 2. In Section 3 we show how Hα equivalent widths and fluxes can be measured from the prism plates. In Section 4 we describe a technique for measuring the radial velocities of the emission-line galaxies. In subsequent work, we aim to give results of a survey of many of the nearby rich clusters with $cz<10\,000\,\mathrm{km\,s^{-1}}$.

2 Observations

2.1 ABELL 347 AND ABELL 1367

Data for the two clusters, Abell 347 and Abell 1367, are listed in Table 1. Both clusters are found within larger associations: Abell 347 is one of five clusters which are condensations in the Perseus supercluster (Giovanelli & Haynes 1986); Abell 1367 belongs to the Coma–Abell 1367 supercluster (Gregory & Thompson 1978). Both clusters are thought to be young and dynamically unevolved. Optically and in X-rays, Abell 1367 has an irregular appearance with low central concentration and high spiral fraction. The X-ray luminosity and inferred temperature of the intracluster gas (2.8 ± 1.0 keV; Mushotzky & Smith 1980) are both low suggesting a relatively shallow potential well. Abell 347 has even lower X-ray luminosity and an even higher fraction of spiral galaxies, suggesting this is also a dynamically unevolved cluster.

*For convenience, the combined Hα+[N II] emission will be referred to in what follows as simply the Hα emission.

Table 1. Basic cluster properties.

Property	Abell 347	Abell 1367	Ref.
R.A. (1950)	$02^h\ 22^m.7$	$11^h\ 41^m.9$	1
Dec. (1950)	$41^o\ 39'$	$20^o\ 07'$	1
l	$141^o.2$	$234^o.8$	
b	$-17^o.6$	$73^o.0$	
z	0.0193	0.0215	2
σ_v (km s^{-1}) (N)	586 (19)	832 (75)	2
R_A (arcmin)	89	80	1
Richness class	0	2	1
Cluster type:			
Bautz-Morgan	II-III	II-III	3
Rood-Sastry	C10	F	2
Oemler	...	Spiral-rich	4
L_X (2-6 keV) (ergs s^{-1})	$< 3.16 \times 10^{42}$	2.88×10^{43}	5

References: (1) Abell 1958. (2) Struble & Rood 1982. (3) Bautz & Morgan 1970. (4) Oemler 1974. (5) Kowalski *et al.* 1984. A Hubble constant, H_0=75 km s^{-1} Mpc^{-1}, is assumed.

2.2 PLATE MATERIAL

Observations were obtained using the Burrell Schmidt telescope (61-/94-cm) on Kitt Peak equipped with a 10° dense flint objective prism. This gives a relatively high dispersion of 400 Å mm^{-1} at rest wavelength Hα, yielding a resolution of 4 Å for 1 arcsec seeing. The dispersion direction was orientated N–S. Two exposures of each cluster were made on IIIaF emulsion, hypersensitized by baking at 65°C in forming gas (a mixture of 2 per cent hydrogen and 98 per cent nitrogen gas). The physical plate size is 19.7×19.7 cm^2. A circular RG 630 filter was used for all exposures except one (Abell 347; plate 14559), for which a square RG 645 filter was used. The plate scale of the Burrell Schmidt is 96.6 arcsec mm^{-1}, with a usable field of a 5.1°-diameter circle with the RG 630 filter and a 5.1°×5.1° square with the RG 645 filter. The RG 645 filter is an improvement over the RG 630 filter not only because of its larger area, but also because it effectively blocks the two [O I] night-sky lines at 6300 and 6364 Å (McCarthy & Treanor 1970) thereby reducing background plate fog. The RG 645–IIIaF emulsion combination gives a band-pass which has a full width at half maximum of ~350 Å centred on 6655 Å with a peak sensitivity at ~6717 Å (corresponding to the peak sensitivity of the IIIaF emulsion). The redshift limit beyond which Hα emission is not readily detected is ~12 000 km s^{-1} (Kinman 1984).

Each cluster had one exposure taken with the telescope east of the pier and one with it west of the pier. Reversing the telescope has the effect of reversing the prism, and thus the direction of increasing wavelength on the plate. This is useful both for the measurement of redshifts (see Section 4.2), and for the detection of emission in cases where the galaxy spectrum overlaps the spectrum of an adjacent object. In addition, obtaining two plates is important in order to reject plate flaws and confirm weak emission features. Because of the different filter shapes and the need to use different guide stars for the east and west telescope settings, the fields are not exactly coincident and contain 'overlap' and 'non-overlap' regions for each cluster.

All the spectra were unwidened in order to achieve maximum sensitivity. Since a typical spectrum is physically quite short (~1.5 mm), overlapping spectra are relatively infrequent

Table 2. Objective prism plates.

Plate no.	U.T. Date	Cluster	Plate Centre R.A. (1950.0)	Dec.	Filter	Exposure (min)	Telescope E/W
13046	1981 Dec 16	Abell 347	$02^h\ 21^m.9$	$+41^o\ 20'$	RG 630	120	W
14559	1983 Oct 29	Abell 347	$02^h\ 24^m.7$	$+41^o\ 36'$	RG 645	120	E
14077	1983 Apr 3	Abell 1367	$11^h\ 37^m.9$	$+19^o\ 59'$	RG 630	75	E
14200	1983 May 3	Abell 1367	$11^h\ 41^m.9$	$+20^o\ 00'$	RG 630	120	W

except at low galactic latitudes. The visibility of the Hα emission feature in the galaxy spectra depends critically on the seeing at the telescope during the exposure. Only plates obtained under conditions of good seeing and good transparency have been included in the present study. Details of the exposures are given in Table 2.

2.3 IDENTIFICATION OF EMISSION-LINE GALAXIES

The plates were systematically searched for galaxies showing Hα emission by one of us (CM) using a binocular microscope at low power (~12×). Separate procedures were adopted for the overlap and non-overlap regions of the plate pairs for each cluster. For the overlap region, galaxies were included in the final list of emission objects only if they clearly showed Hα emission on both plates. This criterion was adopted in order to eliminate spurious identifications due to emulsion defects or random clumpiness of the photographic grains. For the non-overlap region of the plate pairs, galaxies were included in the final list of emission objects only if the Hα emission is so obvious as to render any misidentification unlikely. Thus identifications in the non-overlap region do not represent a uniform extension of the survey beyond the overlap region, since they are based on a more conservative criterion for detection of Hα emission. There is one exception to the above criteria, namely A1367 no. 19* in the overlap region of Abell 1367 (*cf.* Table 4, below). Although strong Hα emission is seen on the plate with the longer exposure, on the plate with the shorter exposure the galaxy is only slightly brighter than the plate limit, and no evidence of emission is detected. Some examples of the objective prism spectra of detected emission-line galaxies are shown in Plates 1 and 2.

The emission-line galaxies detected in Hα in Abell 347 and Abell 1367 are listed in order of increasing RA in Tables 3 and 4 respectively. Positions (epoch 1950.0) of the centres of the emission-line galaxies were measured from the PSS prints using a coradograph†, with an estimated accuracy of approximately 3 arcsec in both RA and Dec. The position refers to the centre of the optical image of the galaxy rather than the position of the emission region, since the region of Hα emission is not necessarily coincident with the centre of the galaxy. In fact, in one case (A1367 no. 22) four distinct widely-separated emission knots are visible along the plane of the galaxy, and in another case (A347 no. 4) the emission shows a double structure (*cf.* Plates 1 and 2). The measured positions were used to obtain the object coordinate identifications given in column 2 of the tables. Various catalogue names of the objects are given in columns 3 to 6. These identifications are taken either from Dixon & Sonneborn (1980), the compilation of Markarian galaxies given by Mazzarella & Balzano (1986) or the *IRAS Point Source Catalog* using the galaxy selection criteria defined by Meurs & Harmon (1987). For four galaxies in Abell 1367 there was some uncertainty regarding their identification with galaxies listed by Reiz (1941). In these cases the Reiz identification has been placed in parentheses (*cf.* Table 4, column 6). Galaxies REIZ 1557

† A manual XY measuring machine.

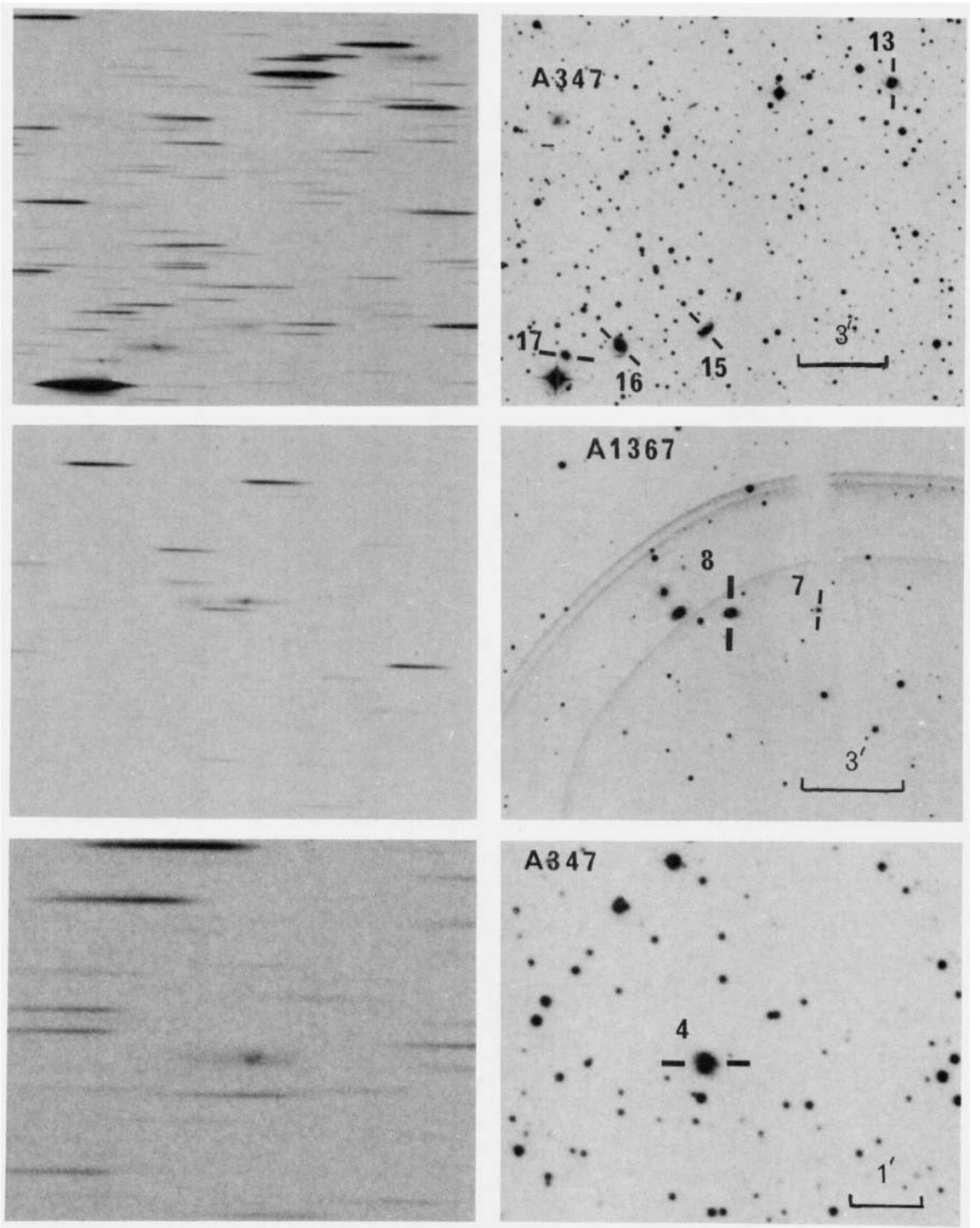

Plate 1. Examples of objective prism spectra of emission-line galaxies. Each field from the prism plate is shown with an enlargement of the PSS field (E plate) to approximately the same scale. North is to the left, and east is at the bottom. The scale of the PSS reproduction is shown in arcmin at the bottom right of each field. Notes on individual objects – A347 nos 13, 15, 16 and 17: the emission for nos 15, 16 and 17 was characterized as 'very diffuse', 'diffuse' and 'very concentrated' respectively. A1367 nos 7 and 8: Markarian 182 and 181 respectively. A347 no. 4: on the original prism plate the emission appears to have a double structure.

[*facing page* 384]

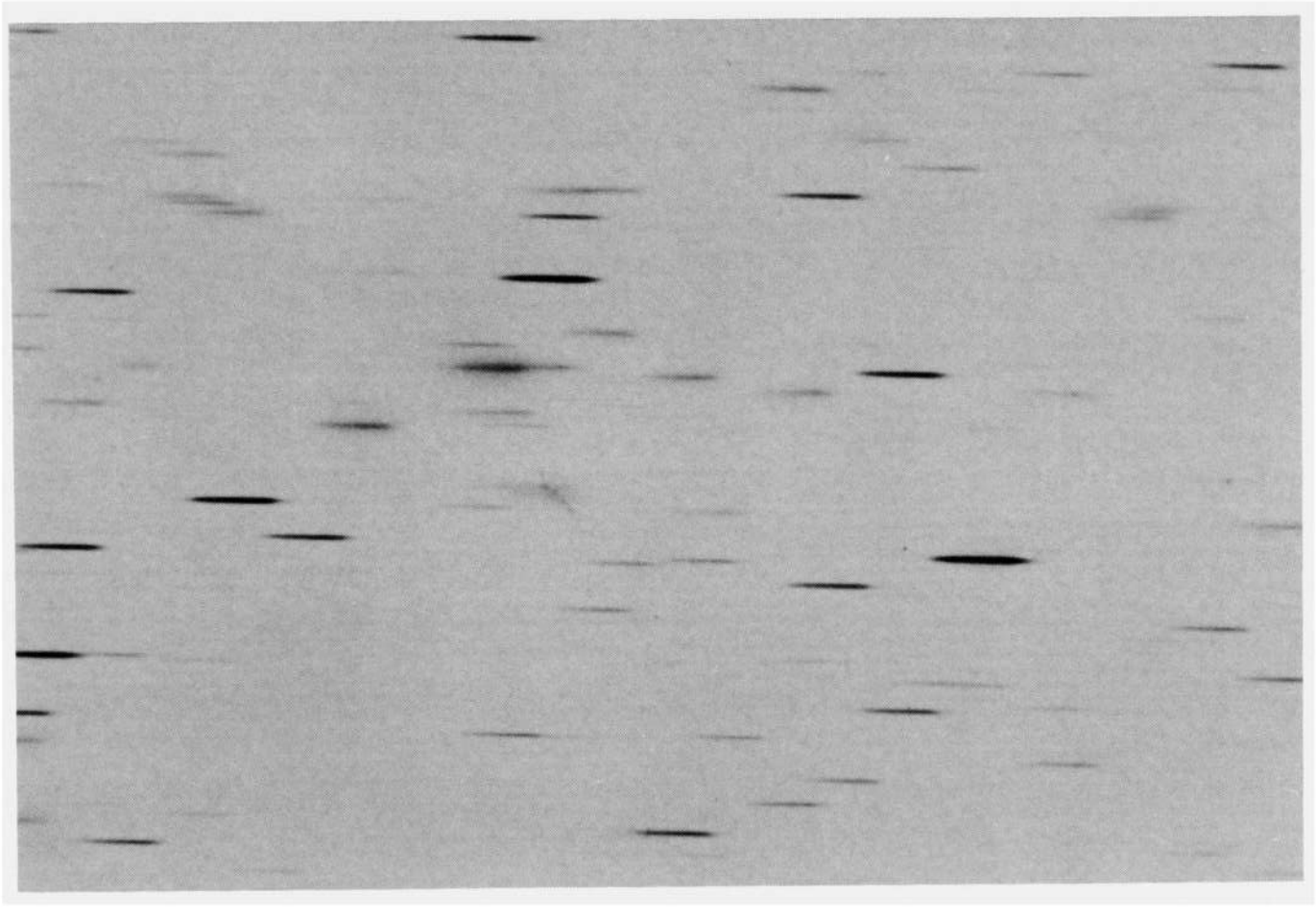

1988MNRAS.232..381M

1988MNRAS.232..381M

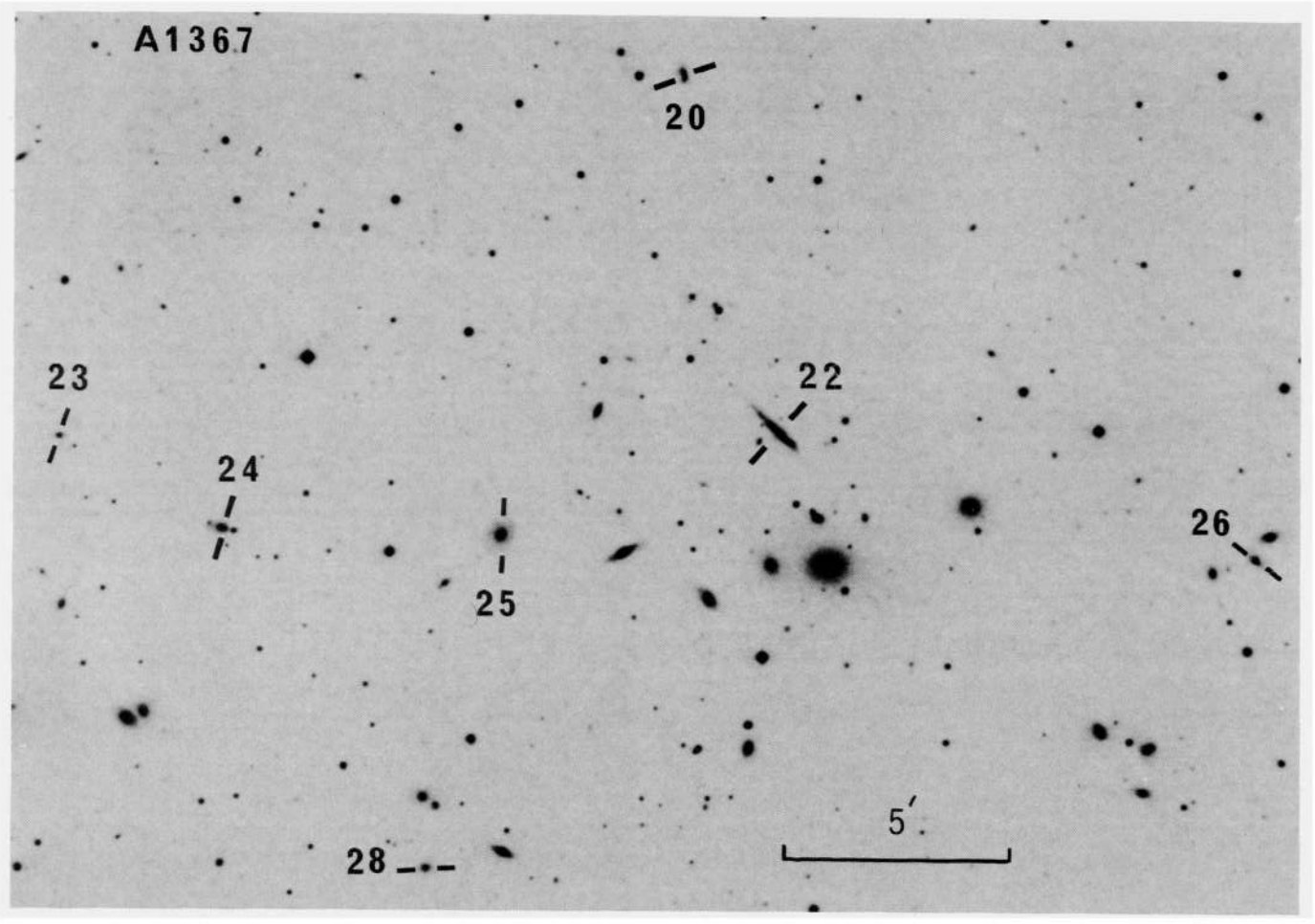

Plate 2. Emission-line galaxies close to the centre of Abell 1367. The field from the prism plate is shown together with the PSS field to approximately the same scale. North is to the left, and east is at the bottom. The scale of the PSS reproduction is shown in arcmin in the bottom right of the field. Galaxy no. 22 (UGC 6697) has four distinct emission knots. The spectrum of galaxy no. 20 is partially overlapped by a star spectrum, but the very strong emission is still visible. The seven emission-line galaxies shown are a subset of 13 emission-line galaxies within ~30 arcmin (≃0.75 Mpc for H_0=75 km s^{-1} Mpc^{-1}) of the cluster centre.

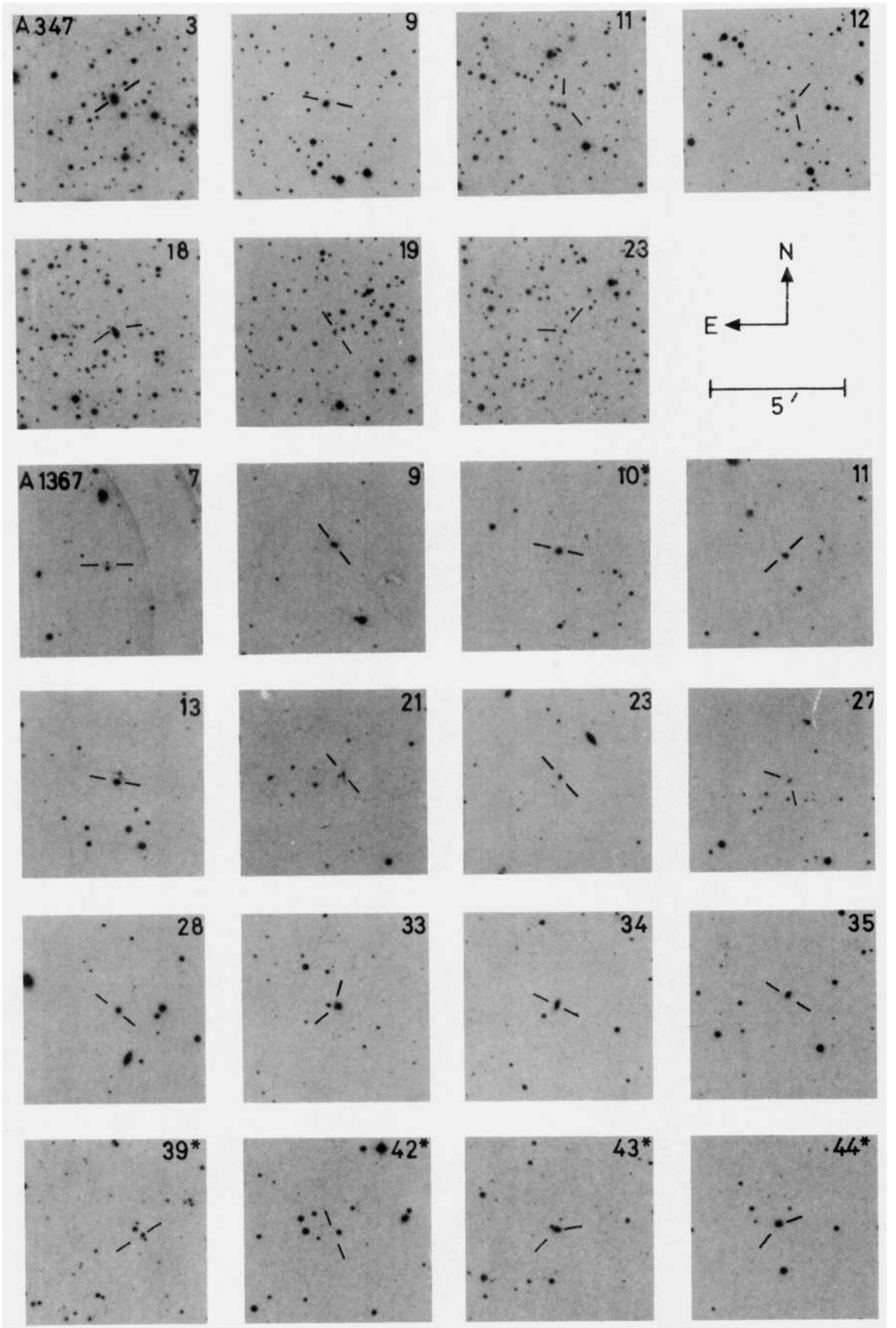

Plate 3. Finding charts for non-CGCG emission-line galaxies in Abell 347 and Abell 1367.

and 1563 are part of a group of Reiz galaxies which have a systematic error in position of −0.2 s in RA and −4 arcmin in Dec.; similarly REIZ 1687 is part of a group which has a systematic error in position of −0.3 s in RA and −8 arcmin in Dec.; finally REIZ 1582 appears to have an error in position of −4.5 arcmin in Dec. Due to confusion caused by a nearby bright star, it is not clear whether IRAS 02244+4145 should be identified with A347 no. 16 or 17. There is the same uncertainty for IRAS 02244+4146. Note that IRAS 11419+2022 is correctly identified with A1367 no. 28 rather than MCG 03-30-083, and that IRAS 11483+2126 is correctly identified with CGCG 127.068 rather than MRK 1461 (=CGCG 127.071=A1367 no. 40*) as given in Lonsdale *et al.* (1985).

In columns 9 and 10 parameters are given to describe the appearance of the emission on the objective prism plates. The visibility parameter (column 9) describes how readily the Hα emission is seen on the plate. This parameter correlates loosely with the Hα flux but not with the Hα equivalent width. In general, the Hα visibility depends on a more complex interaction of several factors such as the spatial distribution of the emission, the apparent size and orientation of the galaxy and the strength of the underlying continuum. Column 10 gives a more straightforward indication of the degree to which the Hα emission is concentrated or diffuse. Notes on individual objects are given below the tables and finding charts of galaxies not listed in CGCG are given in Plate 3.

2.4 COMPARISON WITH OTHER SURVEYS

In the overlap regions of the two clusters, we detect 36 out of 179 CGCG galaxies (20 per cent) in emission whilst 19 out of the 55 emission-line galaxies (35 per cent) are fainter than the CGCG magnitude limit of $m_p=15.7$. Considering only spiral galaxies gives a percentage detection rate which is even higher [see Moss & Whittle (in preparation) for a more detailed analysis]. Thus, rather than detect a small population of unusual or abnormal galaxies, the present technique is able to select a relatively large number of essentially normal galaxies which nevertheless are undergoing moderate (or intense) star formation.

It is also interesting to compare the present survey technique with other surveys which detect emission-line galaxies and related objects, as well as with other surveys which are sensitive to massive star formation. In the overlap region of the two clusters we detect five out of a total of six Markarian galaxies. The one object we do not detect, MRK 637, has a redshift of 19 550 km s^{-1} (Denisyuk, Lipovetskii & Afanasiev 1976) placing the Hα emission well beyond the sensitivity range of the IIIaF emulsion. Thus, on the basis of these admittedly poor statistics, we recover all Markarian galaxies within the possible redshift range.

Wasilewski (1983) has made an objective prism survey for emission-line galaxies covering 825 degree^2 around the north galactic pole. He used the Burrell Schmidt with a 4° prism and unfiltered hypersensitized IIIaJ emulsion. This gives a dispersion of 400 Å mm^{-1} in the Hβ and [O III] (4959, 5007 Å) spectral region. The Hα+[N II] and Hβ/[O III] techniques thus have similar dispersions and limiting continuum magnitudes ($B\sim16$, *cf.* Moss & Whittle, in preparation; Wasilewski 1983), and it is interesting to compare their abilities to detect emission-line galaxies. The two surveys coincide over approximately half the field of Abell 1367. Adopting a conservative declination limit of $\delta\geq20°21'$ for the Wasilewski survey yields an area of 6.5 degree^2 coincident with our two-plate overlap region. In this region 15 emission-line galaxies were detected in Hα whilst the only galaxy detected in Hβ/[O III], Was. no. 26, has a redshift $cz=19\,200$ km s^{-1} (Osterbrock & Shaw 1987), placing it well beyond our detection limit. In the 3.8 degree^2 non-overlap region coincident with the Wasilewski survey, we detect a further 10 emission-line galaxies in Hα including the one galaxy detected in Hβ/[O III] (Was. no. 32=A1367 no. 39*=MRK 1459; $cz=8010$ km s^{-1}). It would seem, therefore, that the present Hα technique is

Table 3. Emission-line galaxies in the field of Abell 347.

No.	Object	Catalogue names				m_p	Type	Emission		$V_\odot$ ($km\ s^{-1}$)
		NGC/IC* UGC	CGCG	MCG IRAS	Other		Ref.	Vis.	Conc.	Refs.
(1)	(2)	(3)	(4)	(5)	(6)	(7)	(8)	(9)	(10)	(11)
1*	021053.5+413837	...	538.034	+07-05-027	...	15.0		S		4375
		...		02109+4138						4
2	021246.4+423531	...	538.037	+07-05-030	KARA 60A	15.6	Sc	MW	VD	
		01738		...			2			
3	021545.9+422051	...	...	...	...	...		S		
		...		02157+4220						
4	021656.9+410246	...	538.043	...	...	15.0		S	DBL	5936
		...		02169+4102						4
5	021727.7+412043	...	538.046	+07-05-039	...	15.3		W	VD	
		...		...						
6	021814.5+423852	...	538.048	+07-05-042	KEEL 52	15.3		MS	D	
		...		02182+4238						
7	021827.9+390744	...	523.029	+06-06-024	KARA 64B	15.3	SB...	W	C	7356
		01813		02184+4907			2			5
8	021942.0+415552	...	538.054	...	KEEL 63	15.7	Sa/b	M	VD	
		...		...			1			
9	022047.9+401306	...	...	...	...	...		S	C	
		...		...						
10	022138.3+414754	...	538.063	...	KEEL 87	15.7	Sb/c	M	VD	
		...	539 009	...			1			
11	022235.7+422538	...	...	...	...	...		MW		
		...		...						
12	022336.2+392558	...	...	...	...	...		W		
		...		...						
13	022337.3+413637	...	539.024	+07-06-020	...	15.0	SBa/b	S		5723
		...		02236+4136			1			3,4
14	022344.4+412757	...	539.025	...	...	15.3	SBa/b	S		4316
		...		02237+4127			1			4
15	022422.0+414227	...	539.029	+07-06-021	...	15.7	Sc/I	MS	VD	
		...		...			1			
16	022425.3+414514	923	539.030	+07-06-022	...	14.4	Sb	S	D	5638
		01915		02244+4145?			1			3,4
17	022427.1+414702	...	539.031	+07-06-023	MRK 1176	15.0		S	VC	5739
		...		02244+4146?						4
18	022456.8+433134	...	...	...	...	...		MS	VD	
		...		...						
19	022716.6+405549	...	...	...	...	...		MW		
		...		...						
20	022806.2+401017	...	539.036	+07-06-027	...	14.7	Sa-b	S	D	
		01988		02281+4010			2			
21	022818.8+400143	...	539.038	...	...	15.7		S		5889
		...		...						4
22	023030.4+410740	...	539.044	...	...	15.3		MS	VD	
		...		...						
23	023206.2+425953	...	...	...	...	...		MS		
		...		...				NC		
24*	023605.7+403927	1003	539.070	+07-06-051	...	12.1	Sc	S		585
		02137		02360+4039			2			2

Table 3–*continued*

References: (1) Fanti *et al.* 1982. (2) Nilson 1973. (3) Hintzen *et al.* 1978. (4) This paper (2.3-m reticon data). (5) Karachentsev 1980.

Notes on individual objects.

No. 4. Emission appears to have a double structure.

No. 7. Interacting with UGC 01810 (Arp 273).

No. 11. Compact galaxy with stellar appearance on PSS.

No. 16. May be IRAS 02244+4146.

No. 17. May be IRAS 02244+4145.

No. 24* Foreground galaxy. Several emission regions visible.

Explanation of columns in Tables 3 and 4.

Column 1. Survey identification number. An asterisk indicates that the object has been detected on only one plate, usually because it lies outside the overlap region of the two plates.

Column 2. Coordinate designation based on 1950.0 coordinates. The format is HHMMSS.S+DDMMSS.

Column 3. Line 1, NGC or IC number; line 2, UGC number (Nilson 1973).

Column 4. Lines 1 and 2, CGCG number and alternate. (Abell 347 – Zwicky & Kowal 1968; Abell 1367 – Zwicky & Herzog 1963).

Column 5. Line 1, MCG number (Vorontsov-Velyaminov & Arhipova 1964); line 2, *IRAS* identification (Lonsdale *et al.* 1985; *Point Source Catalog*).

Column 6. Lines 1 and 2, other identifications taken from Master list of non-stellar optical astronomical sources (Dixon & Sonneborn 1980). Abbreviations used are similar to those used in the Master list, namely ARP – *Atlas of Peculiar Galaxies* (Arp 1966); HOLM – Holmberg (1937); KARA – *Catalogue of Isolated Pairs of Galaxies in the Northern Hemisphere* (Karachentsev 1972); KEEL – Keeler (1900); MRK – (Abell 347 – Markarian *et al.* 1979; Abell 1367 – Markarian 1969; Markarian & Lipovetskii 1974; Markarian & Lipovetskii 1976; Markarian *et al.* 1981); REIZ – Reiz (1941); and VV – *Atlas and Catalogue of Interacting Galaxies* (Vorontsov-Velyaminov 1959).

Column 7. Photographic magnitude taken from CGCG.

Column 8. Lines 1 and 2, morphological type and reference.

Column 9. A visibility parameter (*S* strong, MS medium-strong, M medium, MW medium-weak, W weak, NC no visible continuum) describing the visual appearance of the emission, weighted according to its appearance on both plates.

Column 10. A concentration parameter (VD very diffuse, D diffuse, C concentrated, VC very concentrated, DBL double structure). No entry indicates unremarkable spectral appearance.

Column 11. Lines 1 and 2, heliocentric velocity and reference.

considerably more sensitive than the Hβ/[O III] technique (although the Hβ/[O III] technique has a redshift limit which is twice as great).

There are several possible reasons for this difference in sensitivity. First, Wasilewski widened the spectra by 0.05–0.10 mm corresponding to 5–10 arcsec. The resulting spread in emission, particularly for compact emission regions, lowers the effective contrast against the continuum making the emission less easily visible. (The motivation for widening the spectra is to avoid confusion by spurious plate flaws and grain clumping – a problem we avoid by taking two plates allowing confirmation of emission features.) A related possibility is that the seeing was different for the two surveys. We find that the visibility of the Hα emission depends critically on the seeing, and consequently we have only used plates taken under optimum conditions. Although comparison of seeing estimates is difficult, Wasilewski quotes an average seeing of 3 arcsec which we suspect is somewhat worse than the seeing during our Hα exposures. The most important factor, however, is probably the systematically lower equivalent widths of the Hβ or [O III] emission compared to the Hα+[N II] feature. Using the nuclear spectroscopic observations of Heckman, Balick & Crane (1980) for a sample of normal galaxies, we find mean ratios W_λ(Hα+[N II])/W_λ(Hβ)~10; and W_λ(Hα+[N II])/W_λ([O III])~6 with only moderate scatter and no strong dependence on Hubble type. (Note that the ratio for Hβ is effectively a lower limit since the values were corrected for stellar absorption.) This suggests that for most galaxies the global equivalent width of the Hα+[N II] feature is also several times greater than the global equivalent width of the Hβ or [O III] emission features, and is consequently more easily detected. This would imply that galaxies detected by objective prism techniques at Hβ and [O III] tend to have relatively

Table 4. Emission-line galaxies in the field of Abell 1367.

No.	Object	Catalogue names				m_p	Type	Emission		$V_\odot$ ($km\ s^{-1}$)
		NGC/IC*	CGCG	MCG	Other		Ref.	Vis.	Conc.	
		UGC		IRAS						Refs.
(1)	(2)	(3)	(4)	(5)	(6)	(7)	(8)	(9)	(10)	(11)
1*	112823.6+204441	701*	126.074	+04-27-051	ARP 197	14.7	SB...pec	S	D	6155
		06503		11284+2044	VV 3A		4			5
2*	112826.7+203041	...	126.075	+03-29-061	...	15.4		S		
		...		11284+2030						
3*	113107.7+213923	707*	126.091	+04-27-064	REIZ 1281	14.4	S...	S	VD	6575
		06543		11311+2139			4			5
4	113246.6+203519	...	126.103	...	...	15.7		M	VD	
		...		...						
5	113258.2+204655	...	126.104	...	REIZ 1317	15.6	S	S	D	6679
		...		...			5			5
6*	113352.3+215222	3758	126.110	+04-27-073	MRK 739	14.8		S	C	8897
		...		11338+2152	REIZ 1338					14
7	113417.6+201210	...	...	...	MRK 182	...		S		6304
		...		...						13
8	113417.9+201454	...	97.026	+03-30-019	MRK 181	13.9	S pec	S		6187
		06583		11342+2015	REIZ 1361		1			5
9	113430.8+182814	...	...	...	...	...		S	C	
		...		...						
10*	113646.5+222348	...	...	...	...	...		S		
		...		...						
11	113703.1+200902	...	...	...	REIZ 1427	...		W		
		...		...						
12	113711.6+201239	...	97.044	+03-30-031	REIZ 1431	14.2	S...	W	VD	10964
		06625		11371+2012			4			10
13	113841.4+210632	...	...	...	...	...		M		
		...		...						
14	113938.9+201514	...	97.062	...	...	15.5	S pec	MS		7800
		...		...			1			11
15	113948.8+202349	...	97.068	+03-30-051	REIZ 1489	14.7	Sbc	S		5960
		...		11398+2023			1			5
16	113953.7+183639	...	97.067	+03-30-053	HOLM 281A	14.3	Sm	S	VC	918
		06670		11398+1836	REIZ 1491		3			9
17	114000.7+190724	3827	97.070	+03-30-054	REIZ 1495	13.6	Sc	S	D	3226
		06673		11400+1907			3			7,8
18	114009.4+201838	...	97.072	+03-30-055	REIZ 1497	15.0	Sb	W	VD	6334
		...		...			1			11
19*	114020.7+201440	...	97.073	...	REIZ 1500	15.6	Irr	S	D	7275
		...		...			2			5
20	114037.8+201659	...	97.079	...	...	15.7	Irr	MS		7016
		...		...			1			7
21	114056.4+181511	...	...	...	...	...		MS		
		...		...						
22	114113.0+201455	...	97.087	+03-30-066	...	14.3	S pec	S		6649
		06697		11412+2014			1			10
23	114113.2+203135	...	...	...	REIZ 1523	...		MS	VC	
		...		...				NC		
24	114122.6+202749	...	97.092	...	REIZ 1528	15.5	I/S pec	S		6497
		...		...			2			7
25	114123.3+202119	3840	97.091	+03-30-070	REIZ 1531	14.7	Sbc	S		7367
		06702		11413+2021			1			5

Table 4–*continued*

No.	Object	Catalogue names				m_p	Type	Emission		V_e ($km\ s^{-1}$)
		NGC/IC*	CGCG	MCG	Other		Ref.	Vis.	Conc.	Refs.
		UGC		IRAS						
(1)	(2)	(3)	(4)	(5)	(6)	(7)	(8)	(9)	(10)	(11)
26	114126.3+200346	...	97.093	...	...	15.5	S pec	MS		4924
		...		...			1			2
27	114138.2+193653	...	...	...	...	...		MW		
		...		...						
28	114156.5+202305	...	...	...	...	...		MS		
		...		11419+2022						
29	114212.2+200304	...	97.114	+03-30-087	...	15.4	pec	S		8522
		...		...			1			7
30	114216.9+194356	3859	97.122	+03-30-091	REIZ 1555	14.9	S pec	S		5466
		06721		11423+1943			1			11
31	114219.4+200316	...	97.125	+03-30-092	...	15.6	pec	MS		8245
		...		...			1			2
32	114230.0+214123	...	127.046	...	(REIZ 1557)	15.6	S	S	D	7814
		...		11424+2141			5			5
33	114239.3+215517	...	...	...	...	...		S		
		...		...						
34	114244.3+213658	...	...	...	MRK 1454	...		M		7730
		...		...	(REIZ 1563)					15
35	114250.0+205315	...	...	...	...	...		W		
		...		...						
36	114313.3+205425	...	127.049	...	REIZ 1582	15.5		S		7061
		...		...						5
37	114324.4+204259	732*	127.051	+04-28-050	HOLM 290B	15.1		S		
		...		...	REIZ 1591					
38	114411.2+213259	...	127.055	+04-28-054	MRK 640	15.1		S		6665
		...		...	REIZ 1607					12
39*	114530.4+220617	...	...	...	MRK 1459	...		S		8010
		...		...						16
40*	114820.4+212525	...	127.071	+04-28-066	MRK 1461	15.4		S		6386
		...		...	REIZ 1683					6
41*	114839.7+211648	...	127.074	+04-28-070	MRK 1463	15.0		S		3358
		...		...	(REIZ 1607)					6
42*	114852.5+213458	...	...	...	...	...		S		
		...		...						
43*	114926.4+205615	...	...	...	...	...		S		
		...		...						
44*	114949.6+203613	...	...	...	REIZ 1712	...		S		
		...		...						
45*	115139.4+201821	...	97.180	...	REIZ 1755	15.6	S	S	D	6187
		...	98.002	...			5			5

References: (1) Sullivan, Bothun & Bates 1981. (2) Tifft 1978. (3) Gregory & Thompson 1978. (4) Nilson 1973. (5) Bothun *et al.* 1985. (6) Markarian *et al.* 1984. (7) Dickens & Moss 1976. (8) Kirshner 1977. (9) Fisher & Tully 1981. (10) Huchra *et al.* 1983. (11) Giovanelli & Haynes 1985. (12) Denisyuk *et al.* 1976. (13) Denisyuk *et al.* 1974. (14) Petrosyan, Saakyan & Khachikyan 1979. (15) Markarian *et al.* 1985. (16) Wasilewski 1983.

Notes on individual objects.

No. 17. [S II] emission ($\lambda\lambda$ 6717, 6731 Å) possibly visible.

No. 20. On plate 14200, emission is partially obscured by a star spectrum.

No. 22. Four distinct emission knots are visible, which correspond to the emission regions, $A_1+A_2+A_3$, A_4, B_2 and C_1+C_2 respectively in the Hα map of this galaxy given by Gavazzi *et al.* (1984).

No. 24. Bright component of double system.

No. 30. Extended emission along plane of galaxy.

No. 37. S component of double galaxy system.

Column descriptions as for Table 3.

strong emission and/or relatively high excitation compared to those detected at Hα, and are consequently rarer.

Another quantity which has been shown to correlate well with the current massive star formation is the far infrared emission (de Jong *et al.* 1984; Dennefeld *et al.* 1986). To what extent do the present Hα survey and the *IRAS* survey detect similar galaxies? *IRAS* sources falling inside the overlap region of both clusters were selected from the *Point Source Catalog* using the galaxy selection criteria defined by Meurs & Harmon (1987). Of the 26 CGCG galaxies detected by *IRAS*, 17 (65 per cent) are detected in Hα (increased to 71 per cent if the two *IRAS* galaxies whose spectra overlap star spectra are excluded). A further 21 CGCG galaxies are detected in Hα which are not detected by *IRAS*. Below the CGCG limit a further 18 galaxies are detected in Hα and 10 galaxies are detected by *IRAS*, with only two galaxies in common. Of the non-CGCG *IRAS* galaxies, two have spectra overlapping nearby stars, one (MRK 637) has a redshift of 19 550 km s^{-1} and the remaining seven are faint (estimated magnitudes 16–19) and at least some are likely to have redshifts greater than the 12 000 km s^{-1} limit of the Hα prism technique. Thus, of all *IRAS* galaxies which are potentially detectable by the Hα prism technique ($cz \leqslant 12\,000$ km s^{-1} and a spectrum clear of stellar overlap), 60–80 per cent are in fact recovered by the Hα prism technique, whilst the number of emission-line galaxies detected is approximately twice the number detected by *IRAS*.

2.5 DETECTION LIMITS

In the overlap region of Abell 1367, Kennicutt *et al.* (1984) obtained wide-aperture Hα photometry of 15 galaxies. Of these, we detect nine. Fig. 5(a) and (b) show the distributions of equivalent width and flux of the detected and undetected galaxies. There is a relatively sharp cut-off in equivalent width at $W_\lambda = 20$ Å. For $W_\lambda \leqslant 20$ Å we detect one out of six galaxies; for $W_\lambda > 20$ Å we detect eight out of nine galaxies. The flux cut-off is less clear. For $f \leqslant 10^{-13}$ erg cm^{-2}s^{-1} we detect two out of six galaxies; for $f > 10^{-13}$ erg cm^{-2}s^{-1} we detect seven out of nine galaxies. Since both the equivalent width and flux are relevant to the probability of detection of the Hα emission, a combined parameter, $W_\lambda \times f$, may be used to characterize ease of detection. Fig. 5(c) shows the distribution of $W_\lambda \times f$ for detected and undetected galaxies. A clear cut-off is evident: for $W_\lambda \times f \leqslant 3 \times 10^{-12}$ Å erg cm^{-2}s^{-1} we detect one out of seven galaxies; for $W_\lambda \times f > 3 \times 10^{-12}$ Å erg cm^{-2}s^{-1} we detect eight out of eight galaxies. We conclude that the approximate detection limits of the survey in Hα+[N II] equivalent width and flux are $W_\lambda = 20$ Å and $f = 10^{-13}$ erg cm^{-2}s^{-1}, while a more precise limit is $W_\lambda \times f = 3 \times 10^{-12}$ Å erg cm^{-2}s^{-1}. Finally we note that these estimates of the detection limits may be rather conservative since one exposure of Abell 1367 was relatively short (75 min, *cf.* Table 2).

3 Measurement of global Hα equivalent widths and fluxes

3.1 PLATE DIGITIZATION

The objective prism spectra were digitized using the KPNO PDS microdensitometer. A 20 μm square spot was stepped at 10 μm intervals to give a raster scan of 200 samples in the dispersion direction and between 15 and 65 samples in the perpendicular direction (depending on the width of the spectrum). The photographic density was converted to relative intensity using calibration spots obtained by taking two 20 min sensitometer exposures using the same filter-emulsion combinations as used for the observations. Although only approximate, this conversion was found to be sufficiently accurate for the present purposes. The digitized spectra were summed perpendicular to the dispersion direction. The sky level was determined from the ends of the

spectra and subtracted. In two cases, A1367 nos 22 and 30, the Hα emission is distributed along the galaxy image and tilted with respect to the direction of summation. For these galaxies, the individual spectra were shifted before summing to compensate for the spread of the emission, thereby superposing the Hα emission in the final spectrum.

3.2 EQUIVALENT WIDTHS

It was possible to measure equivalent widths of the combined Hα+[N II] emission from the digitized one-dimensional objective prism spectra in 55 per cent of the sample of emission-line galaxies. Galaxies which were not measured usually had emission or continuum which was either too faint or too diffuse to be measured reliably. For galaxies which could be measured, the continuum outside the emission line was fitted by a polynomial. Since the prismatic dispersion varies quite rapidly with wavelength, it is necessary to know the wavelength of the Hα emission in order to convert equivalent width in pixels to Ångstroms. A comparison of the prism spectra with the combined filter–emulsion response shows that the general spectral shape is almost completely determined by the filter–emulsion combination, with the peak in the continuum coinciding with the peak sensitivity of the IIIaF emulsion (~6717 Å). Thus the position of the peak of the continuum, together with the dispersion curve of the 10° prism (taken from the Operation Manual for the Burrell Schmidt telescope) can be used to set the wavelength scale. Estimates of the errors in the equivalent width were made based on the uncertainty of the continuum fit. These error estimates agreed well with the plate-to-plate differences for individual galaxies and will be used in what follows as estimates of the internal error. The errors are typically in the range 10–20 per cent.

In Table 5 and Fig. 1, a comparison is made between the equivalent widths measured photometrically by Kennicutt *et al.* (1984) and those measured from the objective prism spectra for the emission-line galaxies in Abell 1367. For the six galaxies which have measurements in

Table 5. Comparison of equivalent width and flux measurements for emission-line galaxies in Abell 1367.

A1367	CGCG	This paper		Kennicutt et al.	
ELG no.	no.	W_λ(Hα) (Å)	log f(Hα) (erg cm^{-2}s^{-1})	W_λ(Hα) (Å)	log f(Hα) (erg cm^{-2}s^{-1})
(1)	(2)	(3)	(4)	(5)	(6)
1*	126.074	34:	-12.51	34 ± 4	-12.56
8	097.026	95 ± 6	-12.19	88 ± 6	-12.26
15	097.068	22 ± 2	-12.83	44 ± 5	-12.51
18	097.072	-	-13.05:	-	-13.5:
19*	097.073	-	-12.84	-	-12.84
20	097.079	-	-12.54	-	-12.64
22	097.087	64 ± 6	-12.22	61 ± 5	-12.19
25	097.091	17 ± 3	-12.92	23 ± 3	-12.74
30	097.122	39 ± 5	-12.64	46 ± 7	-12.65

Columns 1 & 2: emission-line galaxy number and CGCG number. Columns 3 & 4 : integrated Hα+[N II] equivalent width and flux measured from the objective prism spectra. Columns 5 & 6: as for columns 3 & 4 but measured by Kennicutt *et al.* (1984) using wide aperture photoelectric photometry.

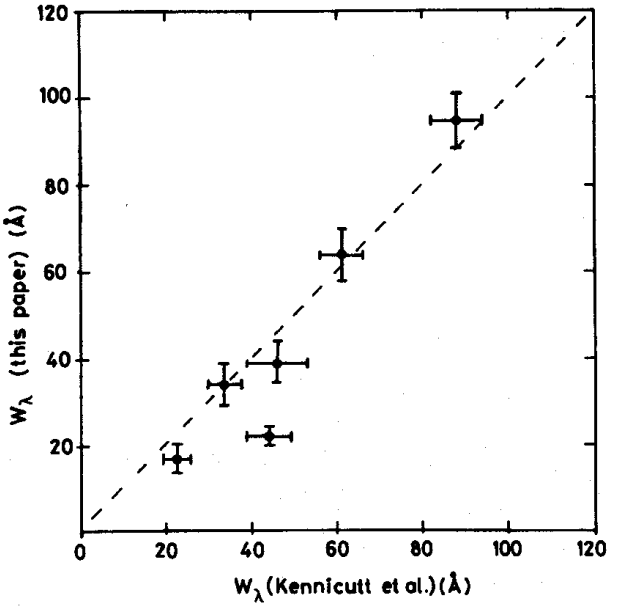

Figure 1. A comparison between values of global equivalent width, W_λ(Hα+[N II]), measured from objective prism spectra (this paper) and from wide-aperture photoelectric photometry (Kennicutt *et al.* 1984). The dashed line shows $y=x$.

common, there is good agreement between the two sets of equivalent widths with the exception of A1367 no. 15, for which the objective prism value is only half the photometric value. Similarly the combined Hα+[N II] flux measured from the objective prism spectra is only half the photometrically measured value (*cf.* Section 3.3). The cause of this disagreement is not yet known, although a possible explanation is that there is substantial diffuse Hα emission spread throughout the disc of this galaxy. Such diffuse emission would not stand out against the galaxy continuum leading to an underestimate of the true flux and equivalent width. Equivalent widths for the combined Hα+[N II] emission for galaxies in Abell 347 and Abell 1367 are given in Tables 6 and 7 respectively.

Table 6. Hα equivalent width and flux measurements for emission-line galaxies in Abell 347.

A 347 ELG no. (1)	CGCG no. (2)	W_λ(Hα) (Å) (3)	log f(Hα) (erg cm^{-2}s^{-1}) (4)	A 347 ELG no. (5)	CGCG no. (6)	W_λ(Hα) (Å) (7)	log f(Hα) (erg cm^{-2}s^{-1}) (8)
1*	538.034	-	-12.95	14	539.025	14 ± 2	-12.85
3	...	45 ± 5	-12.45	15	539.029	-	(-13.06:)
4	538.043	62 ± 8	-12.62	16	539.030	46 ± 3	-12.37
6	538.048	33:	-12.91	17	539.031	61 ± 7	-12.57
8	538.054	52 ± 8	-13.01:	18	...	-	-13.03:
9	...	45 ±10	-12.97	20	539.036	25 ± 4	-12.81
11	...	46:	-13.54	21	539.038	24 ± 4	-13.07
12	...	-	-13.39	22	539.044	-	-12.98:
13	539.024	25 ± 3	-12.74				

Columns 1 & 2: emission-line galaxy number and CGCG number. Columns 3 & 4: integrated Hα+[N II] equivalent width and flux measured from the objective prism spectra. Columns 5–9: same as columns 1–4.

Table 7. Hα equivalent width and flux measurements for emission-line galaxies in Abell 1367.

A1367 ELG no. (1)	CGCG no. (2)	W_λ(Hα) (Å) (3)	log f(Hα) (erg cm^{-2}s^{-1}) (4)	A1367 ELG no. (5)	CGCG no. (6)	W_λ(Hα) (Å) (7)	log f(Hα) (erg cm^{-2}s^{-1}) (9)
1*	126.074	34 ± 4[a]	-12.54[a]	24	097.092	-	-13.06
2*	126.075	23 ± 6	-12.89	25	097.091	20 ± 3[a]	-12.83[a]
3*	126.091	-	-12.65	26	097.093	59:	-12.95
4	126.103	-	-12.88:	27	...	-	-13.23:
5	126.104	-	-12.72	28	...	47 ± 10	-13.14
6*	126.110	74 ± 5	-12.00	29	097.114	79:	-12.82
7	...	-	-12.99	30	097.122	43 ± 5[a]	-12.65[a]
8	097.026	92 ± 4[a]	-12.23[a]	31	097.125	29 ± 4	-13.13
9	...	64 ± 13	-13.10	32	127.046	61 ± 11	-13.05
10*	...	-	-13.04	33	...	47 ± 9	-13.06
11	...	-	-12.97:	34	...	-	-13.22
12	097.044	-	-12.57:	35	...	-	-13.24
13	...	50 ± 10	-13.06	36	127.049	59 ± 4	-12.95
14	097.062	45 ± 10[b]	-13.10[b]	37	127.051	38 ± 3	-12.88
15	097.068	(33)[a]	-12.67[a]	38	127.055	43 ± 6	-12.85
16	097.067	21:	-12.63	39*	...	-	-12.85
17	097.070	59:	-12.14:	40*	127.071	72 ± 12	-12.72
18	097.072	5 ± 3[b]	-13.28:[a]	41*	127.074	45 ± 4	-12.75
19*	097.073	80 ± 12[b]	-12.84[a]	42*	...	85 ± 16	-12.77
20	097.079	145 ± 15[b]	-12.59[a]	43*	...	54 ± 10	-13.00
21	...	-	-12.93	44*	...	36:	-13.19
22	097.087	63 ± 5[a]	-12.21[a]	45*	097.180	-	-13.03:
23	...	-	-12.98				

[a]Mean value from this paper and Kennicutt *et al.* (1984).
[b]Kennicutt *et al.* (1984).

Columns 1 & 2: emission-line galaxy number and CGCG number. Columns 3 & 4: integrated Hα+[N II] equivalent width and flux measured from the objective prism spectra. Columns 5–9: same as columns 1–4.

3.3 FLUXES

Except for a few cases in which the emission was too diffuse or too faint to be measured reliably, the integrated Hα+[N II] intensities for galaxies in the two clusters were measured from the digitized spectra. In order to obtain values of the relative flux, it is necessary to correct these intensities for the variation in the response of the detector system (filter–emulsion combination) as a function of wavelength. This variation in detector response is given by the product of the RG 630 (or RG 645) filter transmittance and the IIIaF sensitivity at each wavelength. Using the galaxy redshift to give the wavelength of the Hα emission, and the calculated detector response at this wavelength, the required corrections were made and relative flux values were obtained. Because the response function has a broad peak at ~6700 Å, these corrections are quite small for most of the galaxies in the clusters: ≤5 per cent for $5000 \leq V_\odot \leq 8000$ km s^{-1}, increasing to 20 per cent at 2000 km s^{-1} and 50 per cent at 9500 km s^{-1} respectively. For Abell 1367, relative flux was converted to absolute flux using measurements in common with Kennicutt *et al.* (1984). For Abell

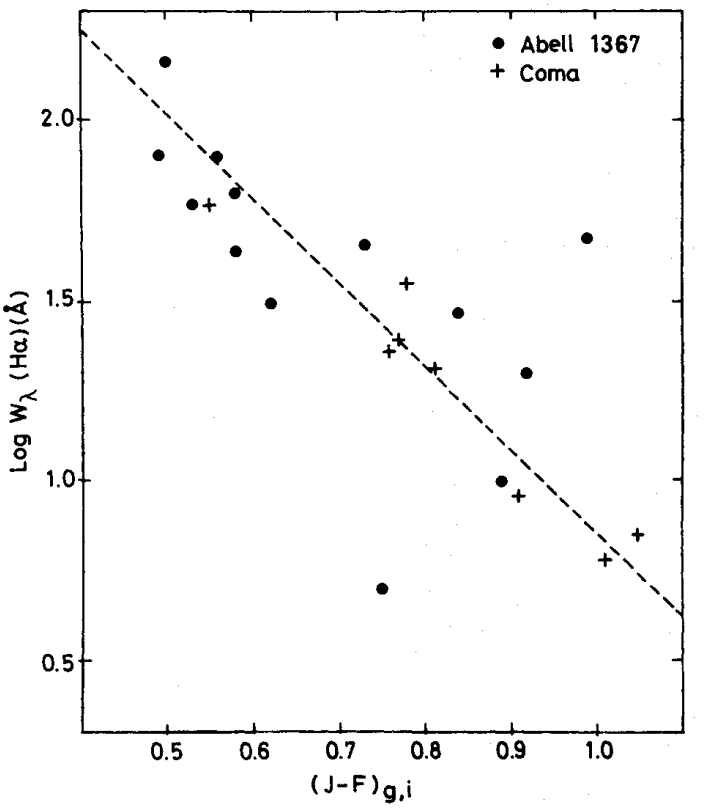

Figure 2. A plot of global Hα+[N II] equivalent width versus (*J–F*) colour corrected for galactic and internal extinction, for galaxies in Abell 1367 and Coma. A linear least-squares fit is shown by the dashed line. This relation is used as part of the procedure in deriving absolute global Hα+[N II] fluxes from the objective prism spectra (see text).

347 there are no photometric measurements of Hα emission, and it is necessary to use an indirect procedure to convert from relative flux to absolute flux, which we now describe.

Ideally a red continuum magnitude would be used to convert the measured Hα equivalent width to an Hα flux. However, the most extensive source of data are blue magnitudes (m_p) from the CGCG which require a colour correction to yield a red magnitude. Fortunately, as originally noted by Cohen (1976), the global Hα equivalent width is itself correlated with the colour of the galaxy and may therefore be used to estimate the colour correction.

Fig. 2 illustrates the correlation between Hα+[N II] equivalent width and corrected galaxy colours for galaxies in Abell 1367 and Coma. Equivalent width measurements were taken from this paper and Kennicutt *et al.* (1984) and (*J–F*) galaxy colours were taken from Butcher & Oemler (1985) and corrected for galactic and internal extinction to yield $(J-F)_{g,i}$. The galactic extinction, $A_{B,g}$, was obtained from RC2 (de Vaucouleurs, de Vaucouleurs & Corwin 1976). The internal extinction, $A_{B,i}$, was obtained using the relations between $A_{B,i}$, log R and Hubble type given in RC2, where R is the apparent axial ratio of the galaxy. Values for R for UGC galaxies were taken from Nilson (1973). For non-UGC galaxies in Abell 1367, major and minor diameters were measured on the same Schmidt plates as were used to determine galaxy types (*cf.* Moss & Whittle, in preparation) and reduced to the UGC system. For non-UGC galaxies in Coma, values of R were obtained from the galaxy inclination, i, given by Bothun *et al.* (1985), and the relation between i and log R given by Aaronson, Mould & Huchra (1980). The effective wavelengths of the *J*- and *F*-bands are λ_J=5000 Å and λ_F=6500 Å respectively (Oemler 1974). Values of the extinction at these wavelengths, A_J and A_F, were obtained from $A_B=A_{B,g}+A_{B,i}$ and the extinction curve given by Savage & Mathis (1979). The colour excess $E(J-F)=A_J-A_F$ was then used to

obtain the corrected colour $(J-F)_{g,i}=(J-F)+E(J-F)$. The colour corrections due to redshift and differences between integrated and asymptotic colour indices are small and have been neglected.

The dashed line in Fig. 2 is a linear least-squares fit to the data [minimizing residuals in $(J-F)_{g,i}$] and was adopted as the mean relation between W_λ and $(J-F)_{g,i}$. It has the form

$$\log W_\lambda = 3.17 - 2.32\,(J-F)_{g,i}. \quad (1)$$

For galaxies in seven clusters we compared J magnitudes, m_J measured by Butcher & Oemler (1985), and corrected CGCG magnitudes, $m_{p,c}$ taken from Kron & Shane (1976). For galaxies with $J-F>0.65$, we find a relation between these magnitudes which is independent of colour and is given approximately by

$$m_{p,c}-m_J=0.33. \quad (2)$$

For the sample of CGCG galaxies in Abell 347 with measured equivalent width, the CGCG magnitude, m_p, was transformed to an F magnitude using the corrections defined in Kron & Shane (1976) and equations (1) and (2). The F magnitude is expected to be proportional to log (f/W_λ) with gradient -2.5, where f is the Hα flux of the galaxy. This is shown in Fig. 3. Points for galaxies in Abell 1367 (filled circles) and Coma (crosses) are in agreement with the expected relation which is indicated by the dashed line. Galaxies in Abell 347 (open circles) require a zero

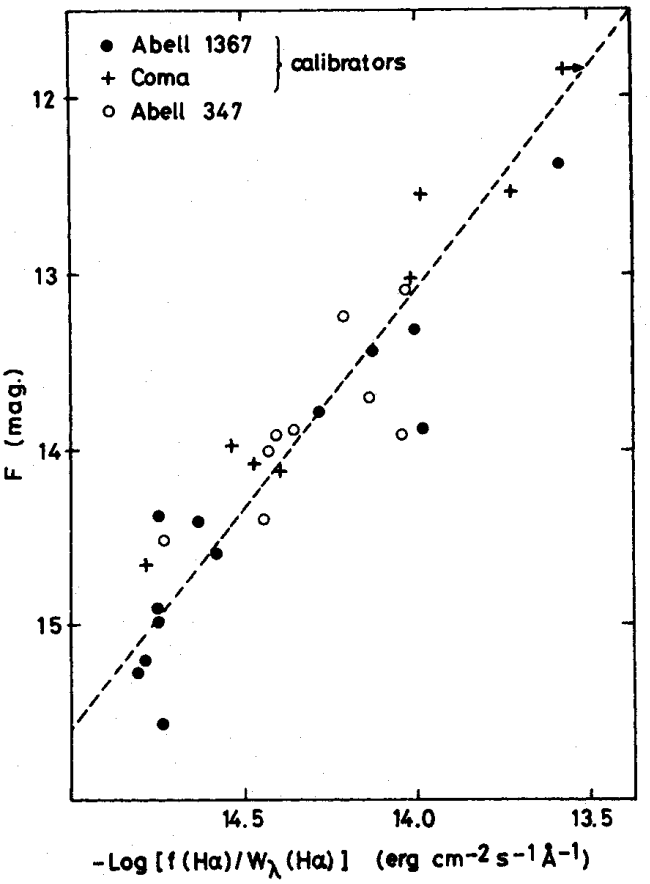

Figure 3. A plot of uncorrected F magnitude versus continuum flux estimator, log $[f(\mathrm{H}\alpha)/W_\lambda(\mathrm{H}\alpha)]$. Galaxies in Abell 1367 (filled circles) and Coma (crosses) have absolute Hα calibration from Kennicutt *et al.* (1984). The dashed line defines the mean relation and has been constrained to have gradient 2.5. Galaxies in Abell 347 (open circles) have been displaced in log $[f(\mathrm{H}\alpha)/W_\lambda(\mathrm{H}\alpha)]$ to fit the relation, thereby defining the conversion from relative to absolute flux.

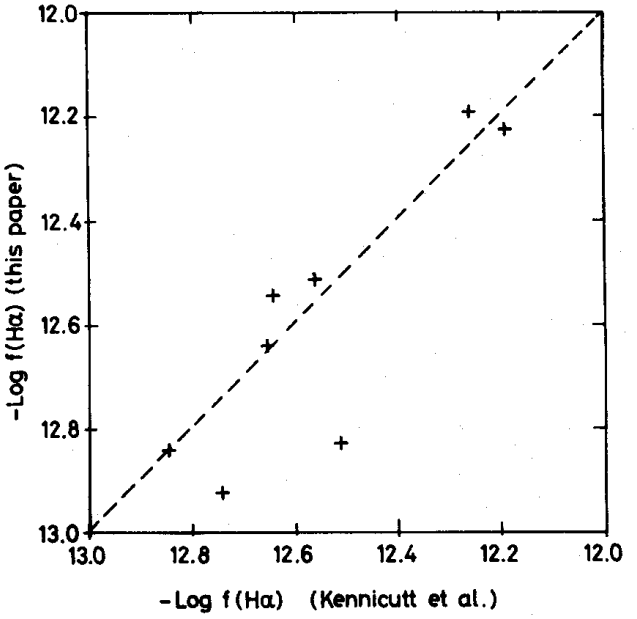

Figure 4. A comparison between values of global Hα+[N II] flux measured from objective prism spectra (this paper) and from wide-aperture photoelectric photometry (Kennicutt *et al.* 1984). The dashed line shows $y=x$.

point shift in log f to bring them into agreement with the other points. This zero-point shift provides the required conversion from relative flux to absolute flux. The estimated uncertainty in the zero point shift is $\Delta(\log f)=0.06$. The estimated random error in the measured values of log f is $\sigma=0.07$ for $-\log f \leqslant 13.0$, and $\sigma=0.09$ for $-\log f > 13.0$.

Table 5 and Fig. 4 present a comparison between values of the combined Hα+[N II] flux for galaxies in Abell 1367 obtained from the objective prism plates, and values obtained photometrically by Kennicutt *et al.* (1984). Of the nine sets of measurements in common, one set (for A1367 no. 18) is uncertain, while the remaining sets are in good agreement with the exception of A1367 no. 15, for which the flux given by Kennicutt *et al.* is almost double that determined from the objective prism spectra (*cf.* Section 3.2). The combined Hα+[N II] fluxes for galaxies in Abell 347 and Abell 1367 are listed in Tables 6 and 7 respectively.

4 Redshifts

4.1 RETICON SPECTRA

Spectra of seven emission-line galaxies in Abell 347 were obtained using the 2.3-m telescope of Steward Observatory, equipped with a Boller & Chivens spectrograph and Reticon dual diode array (Latham 1982). A 300 l mm^{-1} grating gave approximately 14 Å resolution (FWHM) with 3.5 arcsec dual circular apertures separated by 24 arcsec in RA. Wavelength coverage was 3400–7000 Å. Typical integration times were 20 min with He–A comparison spectra taken before and after each galaxy observation.

Table 8 gives the measured features and resulting heliocentric velocity. The estimated external error is 65 km s^{-1}, obtained by comparison of measured velocities with previously determined values (including other objects not presented in Table 8). Note that for the two emission-line galaxies, A347 nos 13 and 16, our measured velocities agree well with those of Hintzen, Oegerle & Scott (1978) while for A347 no. 17 the measured value differs significantly from that of Markarian, Lipovetskii & Stepanyan (1980).

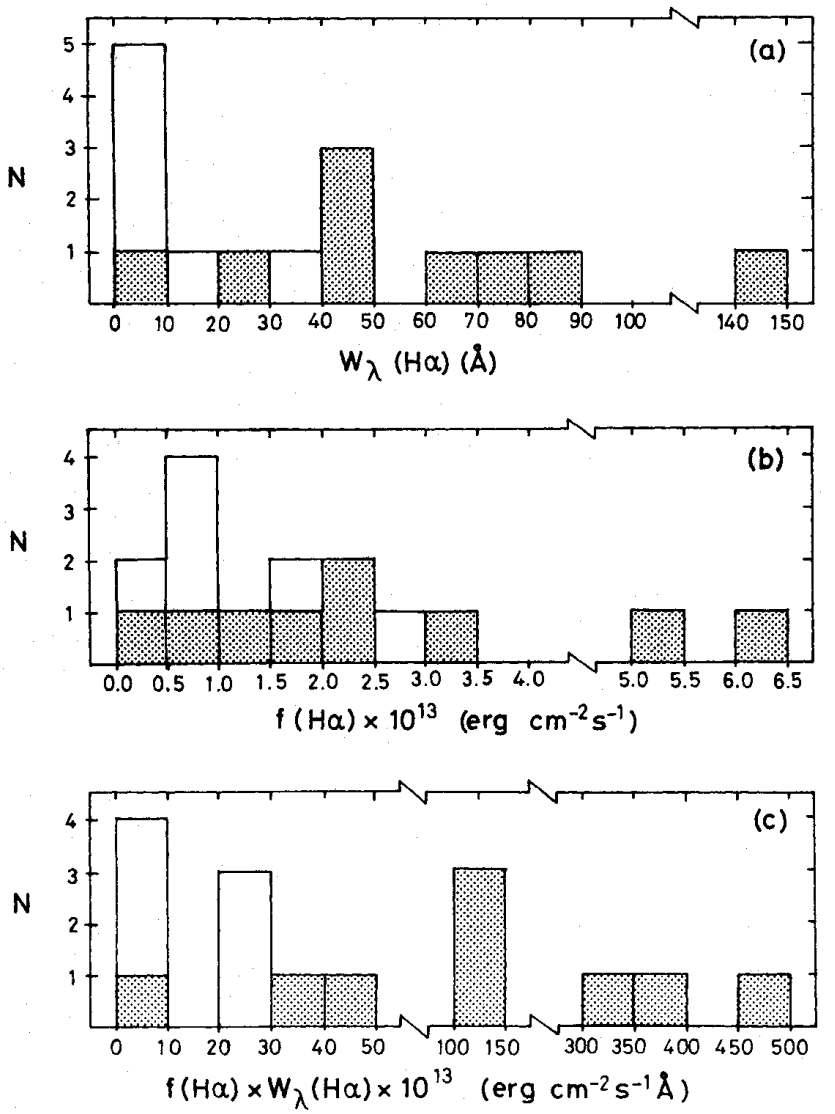

Figure 5. A sample of 15 galaxies in Abell 1367 surveyed for Hα emission by Kennicutt *et al.* (1984). The histograms show the distributions of detected (shaded) and undetected (open) galaxies using the objective prism technique. The distributions of detected and undetected galaxies with Hα equivalent width and flux are shown in (a) and (b) respectively. In (c) the distribution with a combined parameter, $W_\lambda \times f$, is shown.

4.2 OBJECTIVE PRISM SPECTRA

By measuring the position of the Hα feature on the prism plates it is possible to estimate the redshifts of the emission-line galaxies directly. Two techniques have been employed. The first uses a single objective prism plate and is appropriate for emission-line galaxies in the non-overlap regions of the clusters. The second makes use of two plates taken with opposite dispersion directions, and is an inherently more accurate technique. Of the 69 emission-line galaxies identified in Abell 347 and Abell 1367, 38 have previously measured redshifts with which it is possible to calibrate these two techniques.

4.2.1 The single-plate technique

As noted in Section 3.2, the general spectral shape of the continuum of the prism spectra is almost completely determined by the filter-emulsion combination with the peak in the

Table 8. Redshifts of emission-line galaxies in Abell 347 (Reticon measurements).

A 347 ELG no.	CGCG no.	$V_\odot$ (km s^{-1})	Lines measured[a]	U.T. Date of observation
1*	538.034	4375	[OII], Hγ, Hβ, [OIII](4959, 5007 Å), Hα, [NII]	1983 Oct 6
4	538.043	5936	[OII], Hβ, [OIII](5007 Å), Hα.	1983 Jan 21
13	539.024	5635[b]	[OII], Hβ, Hα, [NII].	1983 Sep 7
13	539.024	5811[b]	[OII], K, H, Hβ, NaD, Hα.	1983 Oct 6
14	539.025	4351	[OII], Hβ, Hα, [NII].	1983 Sep 7
14	539.025	4280	Hα, [NII].	1983 Oct 6
16	539.030	5650[c]	[OII], K, H, G, Hβ, Hα.	1983 Jan 21
17	539.031	5739[d]	[OII], Hβ, [OIII](4959, 5007 Å), Hα, [NII].	1983 Jan 21
21	539.038	5822	[OII], K, H, Hβ, [OIII](4959 Å), Hα.	1983 Sep 7
21	539.038	5956	[OII], K, H, Hβ, [OIII](4959, 5007 Å), Hα.	1983 Oct 6

[a]Balmer lines are in emission. [N II] refers to 6584 Å line.
[b]Previous value, 5723 km s^{-1} (Hintzen *et al.* 1978).
[c]Previous value, 5625 km s^{-1} (Hintzen *et al.* 1978).
[d]Previous value, 5338 km s^{-1} (Markarian *et al.* 1980).

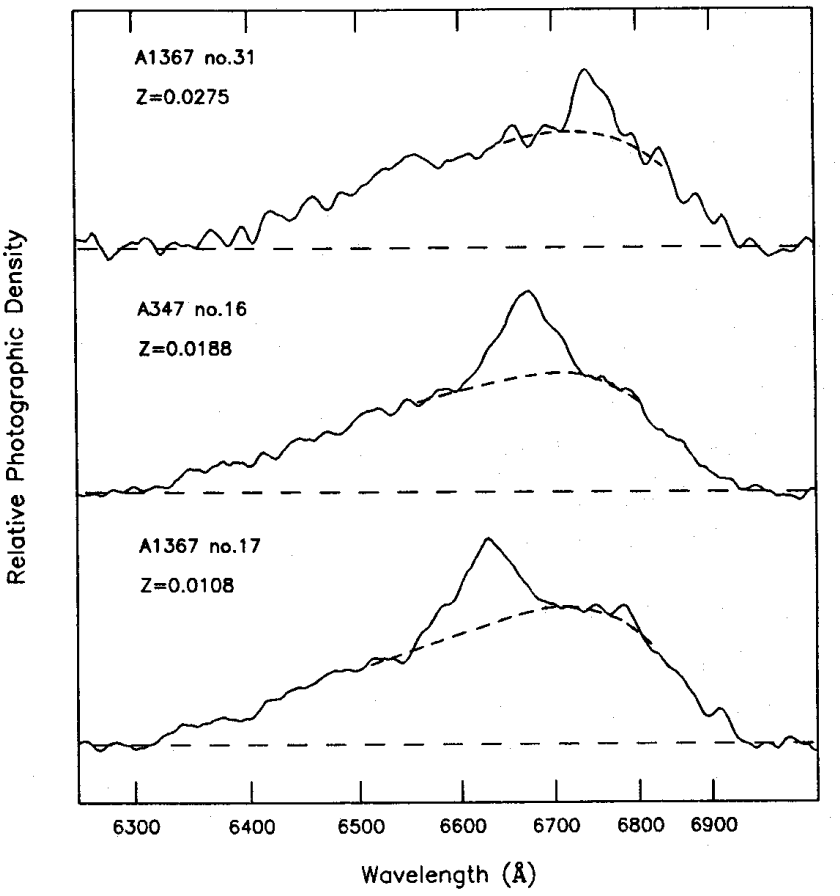

Figure 6. Three examples of digitized objective prism spectra. These spectra were raster scanned in units of photographic density using the Automatic Plate Measuring facility in Cambridge (*cf.* Section 4.2.2). For each spectrum the background sky level was determined from the interpolated mode of the histogram of pixel intensity values, and the sky-corrected values summed perpendicular to the dispersion direction. The approximate position of the continuum under the Hα+[N II] emission is shown by a dashed line. The sky level is indicated by the horizontal dashed line. The change in shift with redshift of the emission line with respect to the continuum peak (at appproximately 6717 Å) is clearly seen. This shift may be used to determine the galaxy redshift.

continuum coinciding with the peak sensitivity of the IIIaF emulsion (~6717 Å). Thus, in principle the offset of the Hα emission feature relative to the continuum peak may be used to estimate the galaxy redshift. Fig. 6 shows three examples of objective prism spectra which illustrate the shift of the Hα emission feature as a function of redshift. It is to be noted that reliable

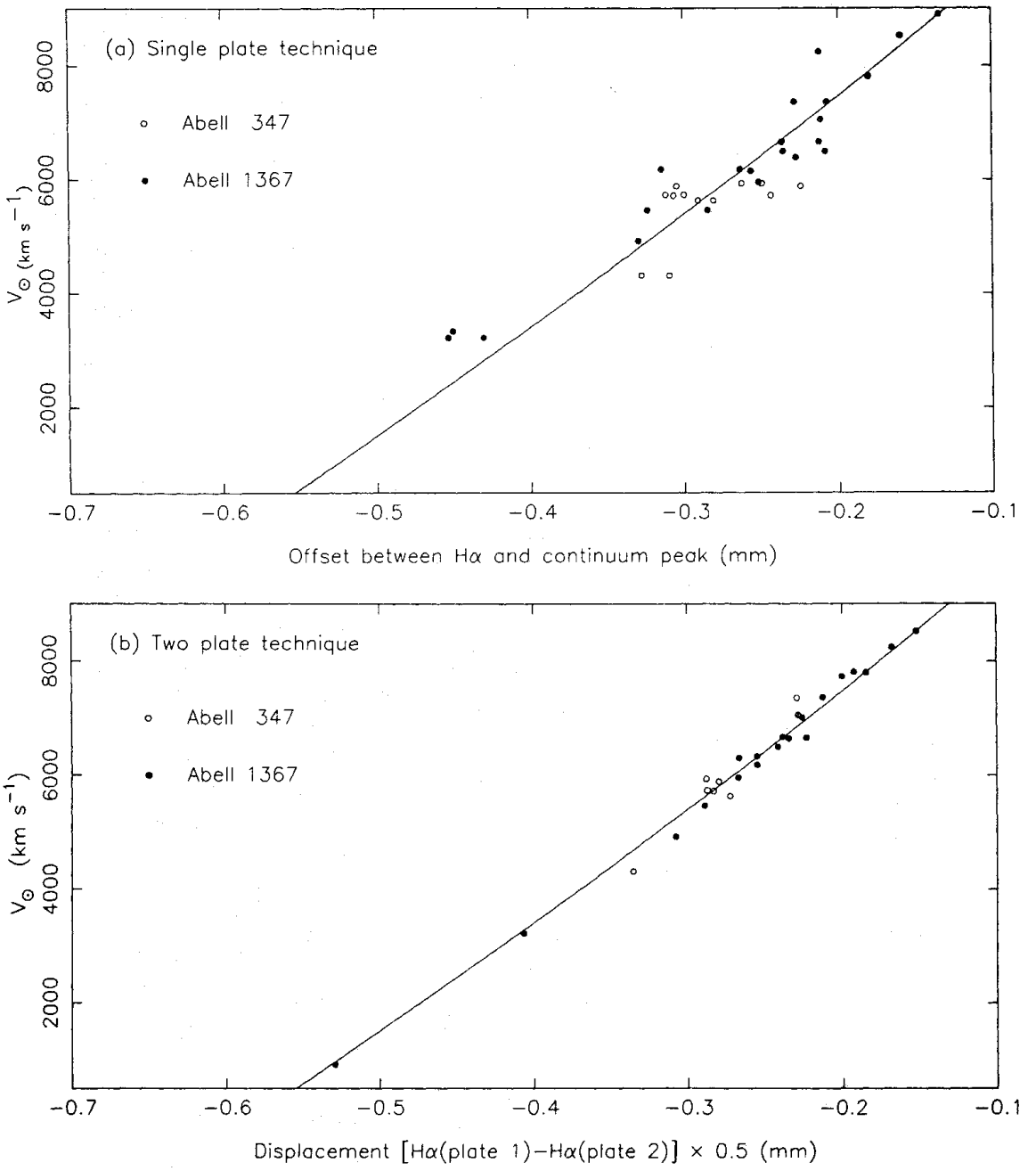

Figure 7. (a) A plot of previously determined radial velocity versus offset between the Hα emission line and the peak of the continuum for galaxies in Abell 347 (open circles) and Abell 1367 (filled circles). For most galaxies, independent measurements were obtained from each of the plates of the plate pair for each cluster, and are plotted as separate points in the diagram. The curve is a relation derived from the dispersion curve of the 10° objective prism, whose zero point is fixed by minimizing the sum of the squares of the residuals in the offset positions. The scatter of the points about the curve corresponds to a (1σ) velocity uncertainty of ~550 km s^{-1}. (b) The same plot as (a), except that radial velocity is plotted against plate-to-plate displacement of the galaxy emission on plates taken with the dispersion direction reversed. The scatter of the points about the curve is now reduced to a (1σ) velocity uncertainty of 205 km s^{-1}.

Table 9. Redshifts of emission-line galaxies (objective prism measurements).

A 347 ELG no.	$V_\odot$ (km s^{-1})	A 1367 ELG no.	$V_\odot$ (km s^{-1})
2	5590:	4	10300:[a]
3	5480	9	6370
5	5920:	10*	(6100)
6	6150:	11	11120[a]
8	6390	13	7310
9	4860	21	2920
10	5680	23	5960
11	5590	27	5700
12	4690	28	7130
15	6740:	33	6580
18	6090	35	7660
19	5270	37	7400
20	5860	42*	(10000)[a]
22	5270:	43*	(8000)
23	4950		

[a]Value obtained by extrapolation beyond the region of calibration.

Velocities were determined using the two-plate technique, except for values enclosed in parentheses which were obtained from a single plate.

redshifts are only obtained if the centres of the Hα and continuum emission distributions are spatially coincident in the direction of the dispersion.

Offsets between the peak of the Hα emission feature and peak of the continuum (derived from a polynomial fit, *cf.* Section 3.2) were measured for those galaxies with sufficiently strong continua. Galaxies in the overlap region contribute two independent offset measurements (one from each plate), while galaxies in the non-overlap region contribute only a single offset measurement. All measurements were considered independently. In Fig. 7(a) the measured offsets are plotted against previously determined radial velocities. The dispersion curve for the 10° objective prism was used to derive a relation between velocity and measured offset, which is also plotted in the figure. The zero point for this relation was determined by minimizing the sum of squares of the residuals in the offset positions. The scatter of the points about this relation corresponds to a (1σ) velocity uncertainty of $\sim$550 km s^{-1}, with no significant dependence on redshift, galaxy magnitude or Hα equivalent width or flux.

Furthermore, all points lie within 3σ of the curve suggesting that, within this uncertainty few, if any galaxies show large systematic errors resulting from a projected physical displacement between the centres of the Hα and continuum emissions. This implies that the distribution of the projected angular displacement between the centre of the Hα emission and the centre of the galaxy continuum (usually the nucleus) has a dispersion $\lesssim$3 arcsec (corresponding to $\sim$550 km s^{-1}). Assuming a random orientation in space gives a deprojection factor of 2 and consequently a physical separation of $\lesssim$2.5 kpc at the distance of the clusters (assuming H_0=75 km s^{-1} Mpc^{-1}). Thus, in general, either the emission originates within 2.5 kpc of the nucleus, or it is distributed approximately symmetrically about the nucleus (for galaxies with diffuse emission).‡

‡One exception is A1367 no. 22 (*cf.* Section 2.3).

New redshift estimates for galaxies in the non-overlap regions of the two clusters have been included in Table 9. They have a 1σ uncertainty of $\sim 550\,\mathrm{km\,s^{-1}}$ (excluding possible systematic effects) and have been enclosed in parentheses.

4.2.2 *The two-plate technique*

Following the method originally developed by Stock & Osborn (1980), it is possible in principle to obtain more accurate redshift estimates by measuring the separation between emission features on two plates taken with opposite dispersion directions. The plate-to-plate separations have first to be corrected for the distortions in position introduced by the objective prism which have a quadratic dependence on object position. The corrected separations in the dispersion direction are simply related to galaxy radial velocity and can be calibrated using galaxies of known redshift. Because this two-plate technique does not rely on measuring the galaxy continuum emission, it has two advantages over the single plate technique. First, faint emission-line galaxies with weak or no observed continuum can still provide redshift measurements. Secondly, it is not necessary to assume that the centre of the Hα emission is spatially coincident with the galaxy continuum emission.

The crucial step in the above method of redshift determination is the correction for distortions in object position introduced by the objective prism. Stock & Osborn used absorption lines in the spectra of reference stars distributed uniformly across the prism plate to monitor and correct for these distortions. In the present case, the spectra have a limited bandpass centred near Hα, and few, if any, absorption features are visible in the stellar spectra on the plates. Consequently this procedure cannot be used. An alternative method (e.g. Hewett *et al.* 1985) is to use object positions on a direct plate to monitor and correct for the distortions in position on the prism plate. This procedure is also unsatisfactory in the present case, both because the galaxies frequently have large angular size which leads to a significant uncertainty in measured position, and also because the position of the Hα emission relative to the galaxy centre is usually unknown. However, as noted in Section 3.2 above, the spectral shape of the continuum is principally determined by the filter–emulsion combination and is independent of the colour of the object. This means that the continuum shape of reference stars distributed across the plate may be used to monitor and correct for distortions in position. This procedure is described below.

About 100 fairly bright, uniformly distributed reference stars were selected in each cluster field. Their equatorial coordinates (correct to ~1 arcsec) and coordinates of the emission-line galaxies were measured on PSS prints using a coradograph measuring machine with a number of SAO stars to define the reference frame. These equatorial coordinates were used as an input list in the subsequent scanning of the pairs of prism plates for each cluster.

The prism plates were scanned using the Automatic Plate Measuring (APM) facility in Cambridge (Kibblewhite *et al.* 1984). The scanning procedure was as follows:

(i) The input list of equatorial coordinates was converted to X, Y positions on the APM plate table using an approximate conversion obtained as follows. The prism plate was aligned on the APM machine and X, Y positions were automatically measured for typically 15 SAO stars. A least-squares solution was obtained for linear relations between X, Y and standard coordinates[§] (ξ, η) for these stars. The coordinate conversion is approximate, both because of uncertainties in the measured positions of the spectra, and also because quadratic terms which model the spatial distortions introduced by the objective prism have been neglected.

(ii) A standard scanning mode was used in which the input list of positions was used to automatically drive the APM to each object position, where a pixel map of the spectrum was

§ i.e. equatorial coordinates projected on to the tangent plane. The tangential point is the plate centre.

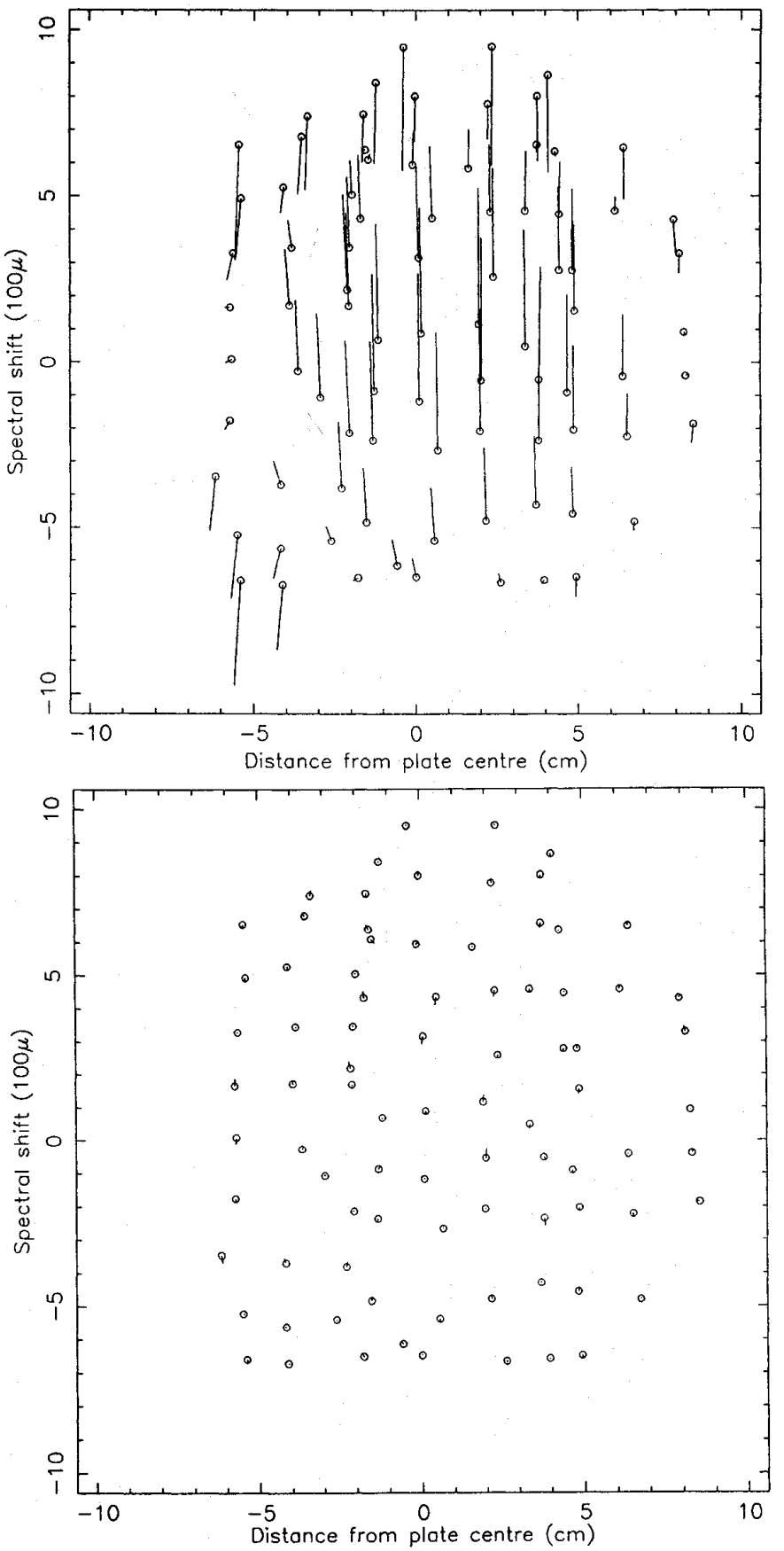

Figure 8.(Top) Plate-to-plate separations of the positions of the objective prism spectra of reference stars for the plate pair for Abell 347. The separations are uncorrected for distortions in position introduced by the objective prism. (Bottom) The same plot, but with subtraction of a modelled (quadratic) distortion.

produced and stored directly on to magnetic tape for subsequent off-line processing. Each map was recorded in units of photographic density and was of size 384×256 pixels, with pixel spacing of 7.6 μm and spot size 10 μm (Gaussian FWHM).

The off-line analysis proceeded as follows.

The position (in pixels) of each reference star spectrum on its pixel map was determined by cross-correlation with an idealized two-dimensional continuum shape. Two such positions were determined for each reference star, one for each plate of the plate pair for the cluster. These positions were then used to compute plate-to-plate separations (in μm) for each reference star as a function of standard coordinates. The computed separations include distortions (quadratic) introduced by the objective prism, small systematic errors (linear) arising from the approximate conversion of X, Y positions to standard coordinates, and random errors due to limitations in the coradograph measuring accuracy. These are plotted in Fig. 8 (top) for the plate pair for Abell 347. The random errors cancel out, while the systematic errors are well modelled by a full quadratic fit of the form,

$$S=A\xi+B\eta+C+D\xi^2+E\xi\eta+F\eta^2. \tag{3}$$

The six constants were separately determined for ΔS_X and ΔS_Y using a standard least-squares method. Subtraction of the modelled distortion results in the residuals depicted in Fig. 8 (bottom). It can be seen that removal of the positional distortions is so successful that remaining residuals are simply individual random errors in determining positions by the cross-correlation method. Systematic errors across the plate are now negligible.

All that now remains is to determine the relative shifts between the Hα emission lines in galaxies for the normal and reverse prism orientation, again using a cross-correlation method, and then to apply the correction computed previously. Because the systematic errors have been reduced to insignificant levels we might expect the resulting errors in radial velocity to be wholly dominated by the information content of the image on the plate. Therefore by using the cross-correlation method (which is the Maximum Likelihood Estimator for this case) to determine the relative Hα shifts, we will have generated the best possible results. Given the average line profile and signal-to-noise ratio in the spectrum it is also fairly straightforward to predict what this minimum error will be (see, for example, Irwin 1985). Making the simplifying assumptions that the line profile is approximately Gaussian with width parameterized by σ_L and that the noise in the spectrum is random with constant variance σ_N^2 we would expect the lower bound on the positional shift variance to be given by

$$\sigma^2 \simeq \sigma_L^2 \frac{\sqrt{16\pi}\sigma_L\sigma_N^2}{I_T^2} \tag{4}$$

where I_T is the total signal (intensity) within the line. Taking σ_L to be ~10 pixels and the signal-to-noise ratio I_T/σ_N as ~100 translates into an expected typical minimum radial velocity error of ~200 km s^{-1}.

In Fig. 7(b) previously determined radial velocities are plotted against plate-to-plate separations for 27 galaxies in the overlap regions of the two clusters. The curve is the same relation as in Fig. 7(a), fitted to the points by the method used previously (*cf.* Section 4.2.1). One point (A1367 no. 12) lies far from the curve and has been omitted. Huchra *et al.* (1983) give a radial velocity for this galaxy of 10 964 km s^{-1}, whereas the objective prism measurement gives 9250 km s^{-1}. With this one exception, the points are in good agreement with the fitted curve and have a (1σ) error of 205 km s^{-1}, which agrees well with the error estimate above. There is no significant dependence of the residuals on velocity, galaxy magnitude, or Hα flux or equivalent width. We conclude that the two-plate technique provides a good method of obtaining accurate estimates of the emission-line

galaxy redshift from objective prism plates in the case of Hα emission. The accuracy obtainable is sufficient not only to establish cluster membership, but also to determine the velocity dispersion of the emission-line galaxies within a cluster.

New redshift measurements for galaxies in the overlap regions of the two clusters are listed in Table 9. They have a 1σ uncertainty of $\sim 205\,\mathrm{km\,s^{-1}}$.

5 Conclusions

A high-dispersion objective prism technique has been used to survey for Hα emission in two rich clusters, Abell 347 and Abell 1367. A total of 69 emission-line galaxies were detected. The aim of the survey is to investigate the effect of environment on star formation in cluster galaxies.

The Hα prism technique is sensitive to narrow-line emission from the nuclei and discs of essentially normal galaxies. Indeed, 20 per cent of CGCG galaxies are detected in emission while approximately 35 per cent of detected galaxies are fainter than the CGCG magnitude limit. The emission-line galaxies were identified by visual inspection of the plates. This also provides some information about the spatial distribution of emission (e.g. concentrated or diffuse). Unfortunately the ability to detect Hα emission is not cleanly defined, since it depends on the interplay of several factors, such as the apparent size and inclination of the galaxy, and the spatial distribution and strength of the emission. In particular, it is possible that diffuse emission spread throughout a large galaxy might escape detection. Nevertheless, it has been possible to establish reasonably clear detection thresholds, with decreases in detection efficiency for global equivalent widths $W_\lambda(\mathrm{H}\alpha+[\mathrm{N\,II}]) \lesssim 20$ Å or global flux $f(\mathrm{H}\alpha+[\mathrm{N\,II}]) \lesssim 10^{-13}\,\mathrm{erg\,s^{-1}\,cm^{-2}}$ or, more exactly, $W_\lambda \times f \lesssim 3\times 10^{-12}$ Å $\mathrm{erg\,s^{-1}\,cm^{-2}}$. The detection efficiency also sharply decreases for galaxies with $cz > 12\,000\,\mathrm{km\,s^{-1}}$ due to the sensitivity cut-off of the IIIaF emulsion at ~6800 Å (Kinman 1984). For the present study, however, this is not a significant limitation since an investigation of global star formation in galaxies must also include accurate morphological information and this necessarily restricts the survey to rich clusters with $cz < 10\,000\,\mathrm{km\,s^{-1}}$.

We have compared the present technique with objective prism methods used in the Markarian and Wasilewski surveys. Allowing for the redshift limit of the survey technique, all Markarian and Wasilewski galaxies in the surveyed regions are recovered, and many additional emission-line galaxies are detected. The present survey is also very efficient at recovering *IRAS* galaxies (between 60 and 80 per cent of potentially detectable *IRAS* galaxies are recovered), whilst the total number of emission-line galaxies is approximately twice that of the *IRAS* sample.

The prism plates were digitized and the global Hα+[N II] equivalent widths for approximately half the emission-line galaxies were measured, giving internal errors of 10–20 per cent. Relative fluxes were also measured and transformed to absolute flux using CGCG magnitudes and an empirically determined colour correction, giving internal rms errors ~15–25 per cent. Comparison with wide-aperture photometric measurements by Kennicutt *et al.* (1984) for a small sample of galaxies in common shows remarkably good agreement (although a more extensive sample for comparison is needed to fully confirm these quantitative methods). Radial velocities can be estimated directly from a single plate with an rms uncertainty $\sim 550\,\mathrm{km\,s^{-1}}$, while a technique using two plates with opposite dispersion directions gives more reliable measurements with rms uncertainty $\sim 200\,\mathrm{km\,s^{-1}}$.

We conclude that the high-dispersion objective prism technique provides an excellent means for surveying nearby rich clusters for galaxies currently forming massive stars. In particular, the technique may be used to measure global Hα+[N II] equivalent widths and fluxes and gives values which compare very favourably with those obtained using wide-aperture photometry. In this paper we have described the technique and methods and presented results on two rich clusters. Some implications of these results have been given by Moss (1988) and will be discussed in more

detail by Moss & Whittle (in preparation). In subsequent work we intend to use the objective prism technique to study many nearby rich clusters and investigate the role of environment on global star formation in cluster galaxies.

Acknowledgments

It is a pleasure to thank the Kitt Peak National Observatory and staff for generous assistance at every stage of this investigation. In particular we are grateful to W. Schoening for help with the observations, and J. Barnes for computer assistance. We would like to thank Steward Observatory for hospitality and the use of the 2.1-m telescope in obtaining the reticon data. T. D. Kinman has taken an interest in this project, and given much advice which we appreciate. CM was supported by the Vatican Observatory Research Group, University of Arizona, during much of the period of this project. MW was supported by a NATO Fellowship while at Steward Observatory, and by Jesus College and the Institute of Astronomy while at Cambridge. The APM facility at the Institute of Astronomy, Cambridge is funded by the Science and Engineering Research Council, and we gratefully acknowledge this contribution to the project. Observations were made with the Burrell Schmidt of the Warner and Swasey Observatory, Case Western Reserve University.

References

Aaronson, M., Mould, J. & Huchra, J., 1980. *Astrophys. J.*, **237,** 655.
Abell, G. O., 1958. *Astrophys. J. Suppl.*, **3,** 211.
Arp, H., 1966. *Astrophys. J. Suppl.*, **14,** 1.
Bautz, L. P. & Morgan, W. W., 1970. *Astrophys. J.*, **162,** L149.
Bothun, G. D., Aaronson, M., Schommer, B., Mould, J., Huchra, J. & Sullivan, W. T., 1985. *Astrophys. J. Suppl.*, **57,** 423.
Butcher, H. R. & Oemler, A., 1985. *Astrophys. J. Suppl.*, **57,** 665.
Cohen, J. G., 1976. *Astrophys. J.*, **203,** 587.
Denisyuk, E. K., Babkin, I. G. & Sinyaeva, N. V., 1974. *Astr. Circ. (USSR) No. 837,* 2.
Denisyuk, E. K., Lipovetskii, V. A. & Afanasiev, V. L., 1976. *Astrofiz.*, **12,** 665.
de Jong, T., Clegg, P. E., Soifer, B. T., Rowan-Robinson, M., Habing, H. J., Houck, J. R., Aumann, H. H. & Raimond, E., 1984. *Astrophys. J.*, **278,** L67.
Dennefeld, M., Karoji, H. & Belfort, P., 1986. In: *Star Forming Dwarf Galaxies and Related Objects,* p. 351, eds Kunth, D., Thuan, T. X. & Tran Thanh Van, J., Editions Frontieres, Gif sur Yvette, France.
de Vaucouleurs, G., de Vaucouleurs, A. & Corwin, H. G., 1976. *Second Reference Catalogue of Bright Galaxies,* University of Texas Press, Austin (RC2).
Dickens, R. J. & Moss, C., 1976. *Mon. Not. R. astr. Soc.*, **174,** 47.
Dixon, R. S. & Sonneborn, G., 1980. *A Master List of Non-stellar Optical Astronomical Objects,* Ohio State University Press.
Dressler, A., Thompson, I. B. & Shectman, S. A., 1985. *Astrophys. J.*, **288,** 481.
Fanti, C., Fanti, R., Feretti, L., Ficarra, A., Gioia, I. M., Giovannini, G., Gregorini, L., Mantovani, F., Marano, B., Padrielli, L., Parma, P., Tomasi, P. & Vettolani, G., 1982. *Astr. Astrophys.*, **105,** 200.
Fisher, J. R. & Tully, R. B., 1981. *Astrophys. J. Suppl.*, **47,** 139.
Gavazzi, G. & Jaffe, W., 1985. *Astrophys. J.*, **294,** L89.
Gavazzi, G. & Jaffe, W., 1986. *Astrophys. J.*, **310,** 53.
Gavazzi, G., Tarenghi, M., Jaffe, W., Butcher, H. & Boksenberg, A., 1984. *Astr. Astrophys.*, **137,** 235.
Giovanelli, R. & Haynes, M. P., 1985. *Astrophys. J.*, **292,** 404.
Giovanelli, R. & Haynes, M. P., 1986. *Astrophys. J.*, **300,** 77.
Gisler, G. R., 1978. *Mon. Not. R. astr. Soc.*, **183,** 633.
Gregory, S. A. & Thompson, L. A., 1978. *Astrophys. J.*, **222,** 784.
Heckman, T. M., Balick, B. & Crane, P. C., 1980. *Astr. Astrophys. Suppl.*, **40,** 295.
Hewett, P. C., Irwin, M. J., Bunclark, P., Bridgeland, M. T., Kibblewhite, E. J., He, X. T. & Smith, M. G., 1985. *Mon. Not. R. astr. Soc.*, **213,** 971.
Hintzen, P., Oegerle, W. R. & Scott, J. S., 1978. *Astr. J.*, **83,** 478.

Holmberg, E., 1937. *Ann. Obs. Lund.*, **6.**
Huchra, J., Davis, M., Latham, D. & Tonry, D., 1983. *Astrophys. J. Suppl.*, **52,** 89.
Irwin, M. J., 1985. *Mon. Not. R. astr. Soc.*, **214,** 575.
Karachentsev, I. D., 1972. *Astrofiz. Issled. Izu, Spets. Astrofiz.*, **7,** 3.
Karachentsev, I. D., 1980. *Astrophys. J. Suppl.*, **44,** 137.
Keeler, J. E., 1900. *Astrophys. J.*, **11,** 325.
Kennicutt, R. C., 1983. *Astrophys. J.*, **272,** 54.
Kennicutt, R. C. & Kent, S. M., 1983. *Astr. J.*, **88,** 1094.
Kennicutt, R. C., Bothun, G. D. & Schommer, R. A., 1984. *Astr. J.*, **89,** 1279.
Kennicutt, R. C., Keel, W. C., van der Hulst, J. M., Hummel, E. & Roettiger, K. A., 1987. *Astr. J.*, **93,** 1011.
Kibblewhite, E. J., Bridgeland, M. T., Bunclark, P. & Irwin, M. J., 1984. In: *Astronomical Microdensitometry Conference,* p. 277, ed. Klinglesmith, D. A., NASA-2317, NASA, Washington DC.
Kinman, T. D., 1979. *Ricerche Astr.*, **9,** 151.
Kinman, T. D., 1984. In: *Astronomy with Schmidt-type Telescopes, IAU Colloq. No. 78,* p. 409, ed. Cappacioli, M., Reidel, Dordrecht, Holland.
Kirshner, R., 1977. *Astrophys. J.*, **212,** 319.
Kowalski, M. P., Ulmer, M. P., Cruddace, R. G. & Wood, K. S., 1984. *Astrophys. J. Suppl.*, **56,** 403.
Kron, G. E. & Shane, C. D., 1976. *Astrophys. Space Sci.*, **39,** 401.
Latham, D. W., 1982. In: *Instrumentation for Astronomy with Large Optical Telescopes, IAU Colloq. No. 67,* p. 259, ed. Humphries, C. M., Reidel, Dordrecht, Holland.
Lonsdale, C. J., Helou, G., Good, J. C. & Rice, W., 1985. *Cataloged Galaxies and Quasars Observed in the IRAS Survey,* Jet Propulsion Laboratory, Pasadena.
McCarthy, M. F. & Treanor, P. J., 1970. *Observatory,* **90,** 108.
Markarian, B. E., 1969. *Astrofiz.*, **5,** 443.
Markarian, B. E. & Lipovetskii, V. A., 1974. *Astrofiz.*, **10,** 307.
Markarian, B. E. & Lipovetskii, V. A., 1976. *Astrofiz.*, **12,** 389.
Markarian, B. E., Lipovetskii, V. A. & Stepanyan, Dzh. A., 1979. *Astrofiz.*, **15,** 201.
Markarian, B. E., Lipovetskii, V. A. & Stepanyan, Dzh. A., 1980. *Astrofiz.*, **16,** 5.
Markarian, B. E., Lipovetskii, V. A. & Stepanyan, Dzh. A., 1981. *Astrofiz.*, **17,** 619.
Markarian, B. E., Lipovetskii, V. A. & Stepanyan, Dzh. A., 1984. *Astrofiz.*, **20,** 419.
Markarian, B. E., Erastova, L. K., Lipovetskii, V. A., Stepanyan, Dzh. A. & Shapovalova, A. I., 1985. *Astrofiz.*, **22,** 215.
Mazzarella, J. M. & Balzano, V. A., 1986. *Astrophys. J. Suppl.*, **62,** 751.
Meurs, E. J. A. & Harmon, R. T., 1987. *Astr. Astrophys.*, preprint.
Moss, C., 1988. In: *Starbursts and Galaxy Evolution, Proc. 22nd Rencontre de Moriond,* ed. Montmerle, Th., in press.
Mushotzky, R. F. & Smith, B. W., 1980. In: *Highlights of Astronomy,* Vol. 5, p. 735, ed. Wayman, P. A., Reidel, Dordrecht, Holland.
Nilson, P., 1973. *Uppsala General Catalogue of Galaxies, Uppsala astr. Obs. Ann.*, **6.**
Oemler, A., 1974. *Astrophys. J.*, **194,** 1.
Osterbrock, D. E. & Shaw, R. A., 1987. Preprint.
Petrosyan, A. R., Saakyan, K. A. & Khachikyan, E. E., 1979. *Astrofiz.*, **15,** 373.
Reiz, A., 1941. *Ann. Obs. Lund.*, **9.**
Savage, B. D. & Mathis, J. S., 1979. *Ann. Rev. Astr. Astrophys.*, **17,** 73.
Stock, J. & Osborn, W., 1980. *Astr. J.*, **85,** 1366.
Struble, M. F. & Rood, H. J., 1982. *Astr. J.*, **87,** 7.
Sullivan, W. T., Bothun, G. D. & Bates, B., 1981. *Astr. J.*, **86,** 919.
Tifft, W. G., 1978. *Astrophys. J.*, **222,** 54.
Vorontsov-Velayminov, B. A., 1959. *Atlas and Catalogue of Interacting Galaxies,* Sternberg Institute, Moscow State University.
Vorontsov-Velayminov, B. A. & Arhipova, V. P., 1964. *Morphological Catalogue of Galaxies,* Part II, Moscow State University.
Wasilewski, A. J., 1983. *Astrophys. J.*, **272,** 68.
Zwicky, F. & Herzog, E., 1963. *Catalogue of Galaxies and Clusters of Galaxies,* Vol. II, California Institute of Technology Press, Pasadena.
Zwicky, F. & Kowal, C. T., 1968. *Catalogue of Galaxies and Clusters of Galaxies,* Vol. VI, California Institute of Technology Press, Pasadena.